Large-Scale Circulations and Water Masses

1. Wind Gyres
2. Pycnocline Stratification and Ventilation
3. Equatorial Currents
4. Antarctic Circumpolar Current (ACC)
5. Meridional Overturning Circulation (MOC)
6. Thermohaline Circulation (THC)
7. Abyssal Circulation
8. Global Water Masses

Connections to Williams and Follows:

Chap. 8: Ocean gyres and intense currents

Chap. 10: Ventillation

Chap. 12: The deep ocean and overturning

Surface Wind-Driven Currents: Gyres, Equatorial flows, and the ACC

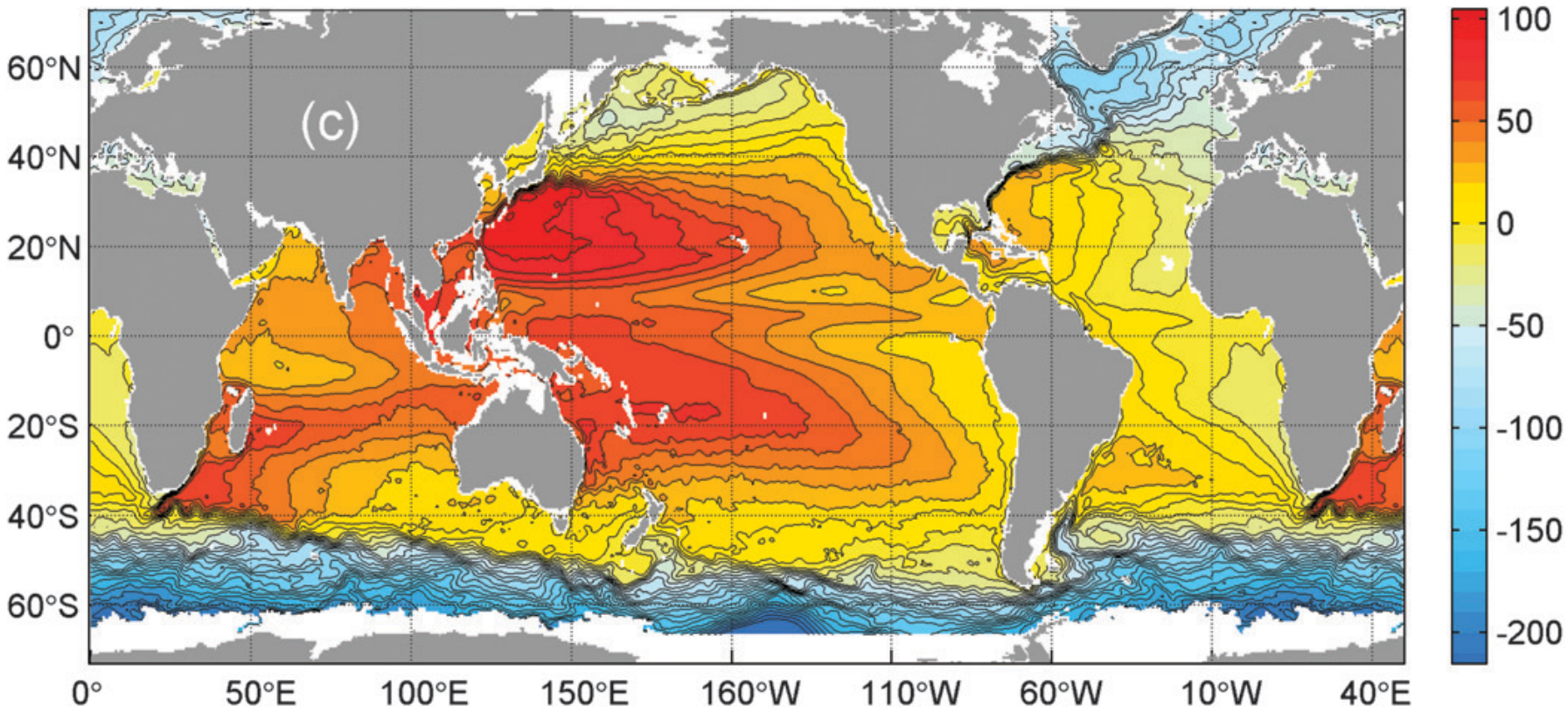

Global mean sea-level $\overline{\eta}$ relative to an iso-surface of Earth's gravitational potential ($i.e.$, dynamic height) in cm with contour interval 10 cm. It is an analysis from altimetry and surface drifters for the period 1993-2002. Geostrophic surface velocity is along the contours. the geostrophic gyres, WBC, ACC, and even equatorial currents are evident. (Note that $\eta/V \to 0$ as $f \to 0$.) This figure is repeated.

1. Ekman Pumping and Wind Gyres

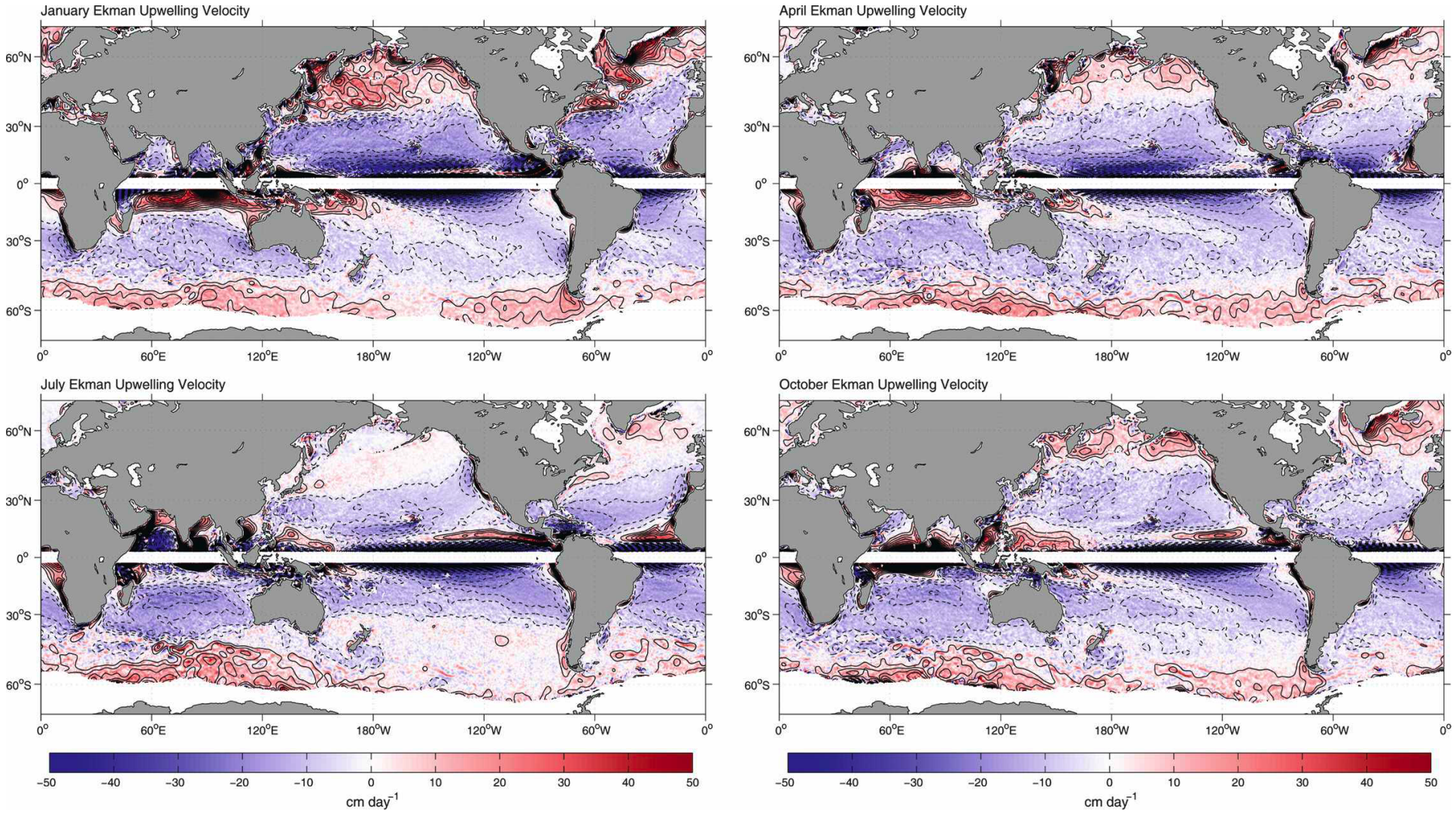

Global mean surface Ekman pumping velocity, $w^s_{ek}(x, y) = curl[\tau^s]/f\rho_0$ [cm d^{-1}], in four seasons from scatterometry. There is subtropical downwelling that leads to subtropical gyres, subpolar upwelling leading to subpolar gyres, equatorial upwellling, upwelling/downwelling south/north of the ACC, and more localized upwelling near the equator and along eastern boundaries.

Concept: Wind curl $\rightarrow$ Ekman pumping $\rightarrow$ interior Sverdrup gyre.

In an extra-tropical surface layer, momentum balance is

$$f(y)\,\hat{\mathbf{z}}\times\mathbf{u} = -g\nabla\eta - \partial_z\overline{\mathbf{u}'w'}\,.$$

$\Rightarrow$ geostrophic and Ekman currents.

Surface layer horizontal transport divergence (locally, ignoring β $etc.$) is

$$\nabla\cdot\int_{-h_{ek}}^{\eta}\mathbf{u}\,dz \approx w_{ek} = \frac{1}{f}\,\mathrm{curl}\left[\frac{\tau}{\rho_0}\right].$$

Below the surface layer, planetary geostrophic vorticity balance is

$$\beta v \approx -f\partial_z w\,,$$

and its vertical integral underneath the Ekman layer (ignoring deep flow) is

$$\beta\int_{-h}^{-h_{ek}} v\,dz = f w_{ek} = \mathrm{curl}\left[\frac{\tau}{\rho_0}\right].$$

This interior v is $\approx$ geostrophic and surface intensified $\Rightarrow$ the pycnocline depth anomaly h_{pyc} is in the opposite sense as w_{ek}; $e.g.$, $w_{ek}<0$ $\rightarrow$ larger h_{pyc}.

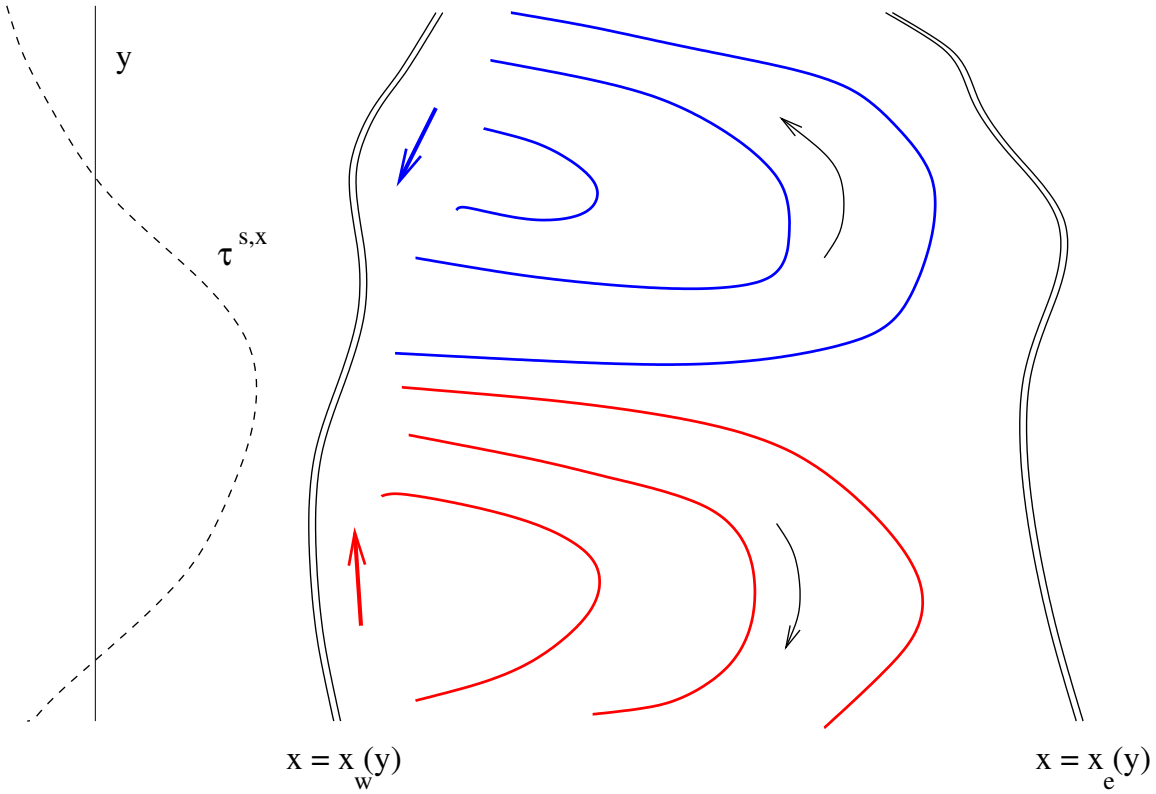

Sketch of Sverdrup gyres in the Northern Hemisphere. A zonal surface stress profile is on the left, with a maximum westerly wind at middle latitudes. The associated Sverdrup transport streamfunction $\Psi^{Sv}(x, y)$ is on the right in an oceanic basin bounded on the west and east by x_w and x_e. Flow is along isolines of Ψ as indicated by the arrows. The subpolar gyre has $\Psi^{Sv} < 0$ (blue contours) and counterclockwise circulation due to the positive wind curl, $-\partial_y \tau^{s,x} > 0$, at high latitudes. The subtropical gyre has $\Psi^{Sv} > 0$ (red contours) and clockwise circulation due to the negative wind curl, $-\partial_y \tau^{s,x} < 0$, in subtropical latitudes, $\sim 15 - 45^o$. The flow near the western boundary is not sketched because it does not satisfy the Sverdrup balance. However, by horizontal transport non-divergence within a bounded basin, there must be return flow for steady-state balance; these occur in western boundary currents (WBCs) as indicated by the colored arrows. This is a repeated figure.

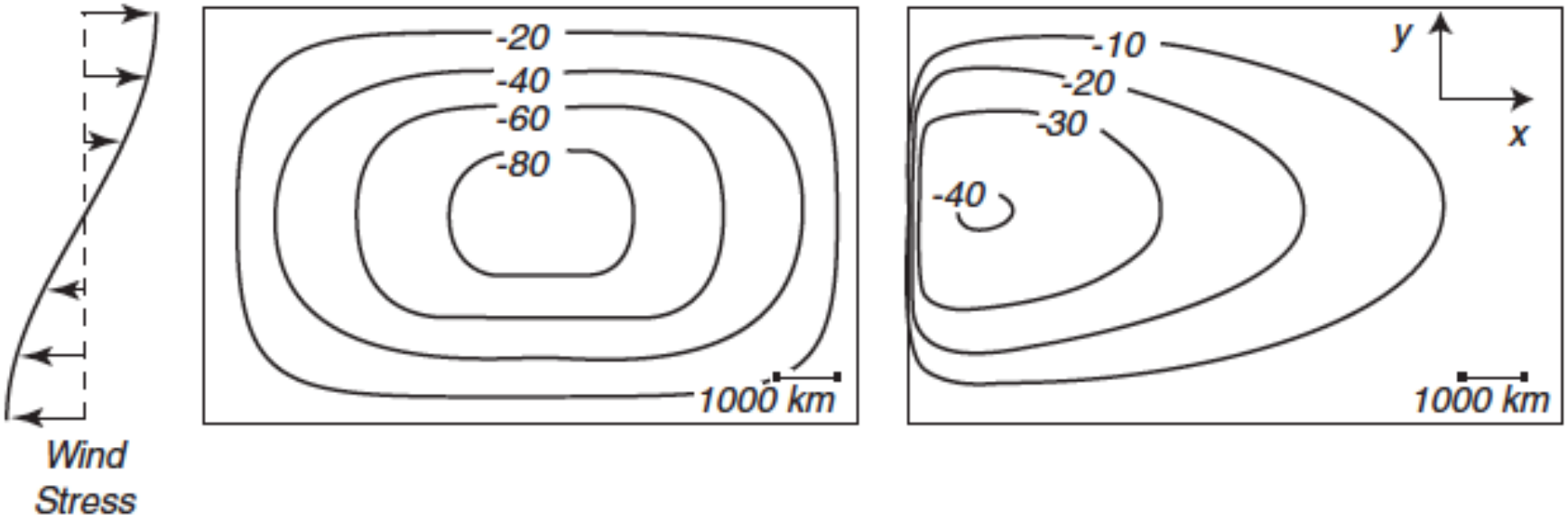

The transport streamfunction Ψ [Sv] for a subtropical gyre in a closed domain (here plotted with the wrong sign; Ψ is a maximum in the middle of an anticyclonic gyre in the Northern Hemisphere). The wind stress $\tau^{s\,x}(y)$ is on the left, and the solution to Stommel's (1948) barotropic model is on the right. The model includes a bottom Ekman drag stress $\tau^b = \rho_0 R\mathbf{T}/h$ as an extension of Sverdrup theory:

$$\frac{R}{h}\nabla^2\Psi + \beta\partial_x\Psi \quad = \tfrac{1}{\rho_0}\,\mathrm{curl}[\tau^s]\,, \qquad \text{with} \quad \Psi = 0 \quad \text{on boundary}\,. \qquad (*)$$

The value of R is empirically chosen to match the width L^w (≈ 100 km) of the Gulf Stream along the east coast of North America. For comparison the middle panel shows an analogous solution except that β is set to zero ($i.e.$, a f-plane model). In this case the interior flow is not Sverdrup flow and there is no WBC. Thus, gyres have their meridional return flow to balance the interior Sverdrup flow along the western boundary because of the direction of Earth's rotation ($i.e.$, $\beta > 0$).

Concept: Why are the Sverdrup-gyre boundary currents on the west?

Given Stommel'smodel (*), consider a boundary-layer correction to Ψ_{sv} to be able to satisfy the boundary condition:

$$\Psi = \Psi_{sv} + \Psi_{bl}\,,$$

where ∂_x when applied to Ψ_{bl} is $\gg L^{-1}$. Then within the boundary layer region,

$$\frac{R}{h}\partial_x^2\Psi_{bl} + \beta\partial_x\Psi_{bl} \approx 0 \qquad \left(i.e., \gg \frac{\beta}{L}\Psi_{sv}\,,\ \frac{\tau_s}{\rho_0 L}\right).$$

Thus,

$$\Psi_{bl}(x) \sim -\,\Psi_{sv}(bdy)\, e^{-\,kx}\,, \qquad k = \frac{\beta h}{R} > 0 \ \ (\gg L^{-1})\,.$$

Only on an west side of a domain can $\Psi_{bl} \to 0$ as x goes into the interior.

This is why Ψ_{sv} is set to zero on an eastern boundary,

$$\Psi_{sv} = -\frac{1}{\rho_0\beta}\int_x^{east\,bdy} \mathrm{curl}[\tau^s]\,dx\,,$$

so that it does not need a boundary-layer correction.

A full mathematical analysis of Stommel's model (*) is in wind_gyre_theory.pdf.

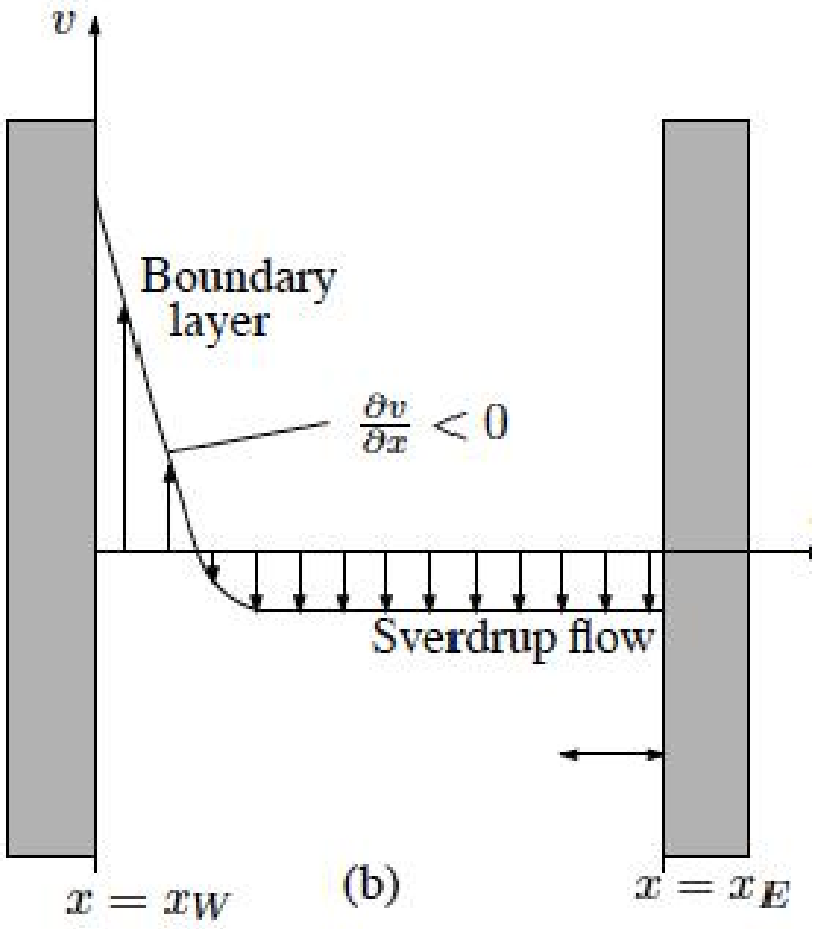

Sketch of the modeled steady, barotropic, meridional velocity $v(x) = h^{-1}\partial_x \Psi$ across a subtropical gyre with curl$[\tau^s] < 0$. The interior velocity is a southward Sverdrup flow and the narrow western boundary current (WBC) is much faster. The zonally integrated meridional transport $\int T^y \, dx$, is zero; $i.e.$, the WBC provides an equal and opposite mass flux to the Sverdrup flow.

In real gyres the WBC is inertial (advectively nonlinear rather than viscous), baroclinic (mainly in and above the pycnocline), unstable (unsteady), and modified by the irregular shape of the basin.

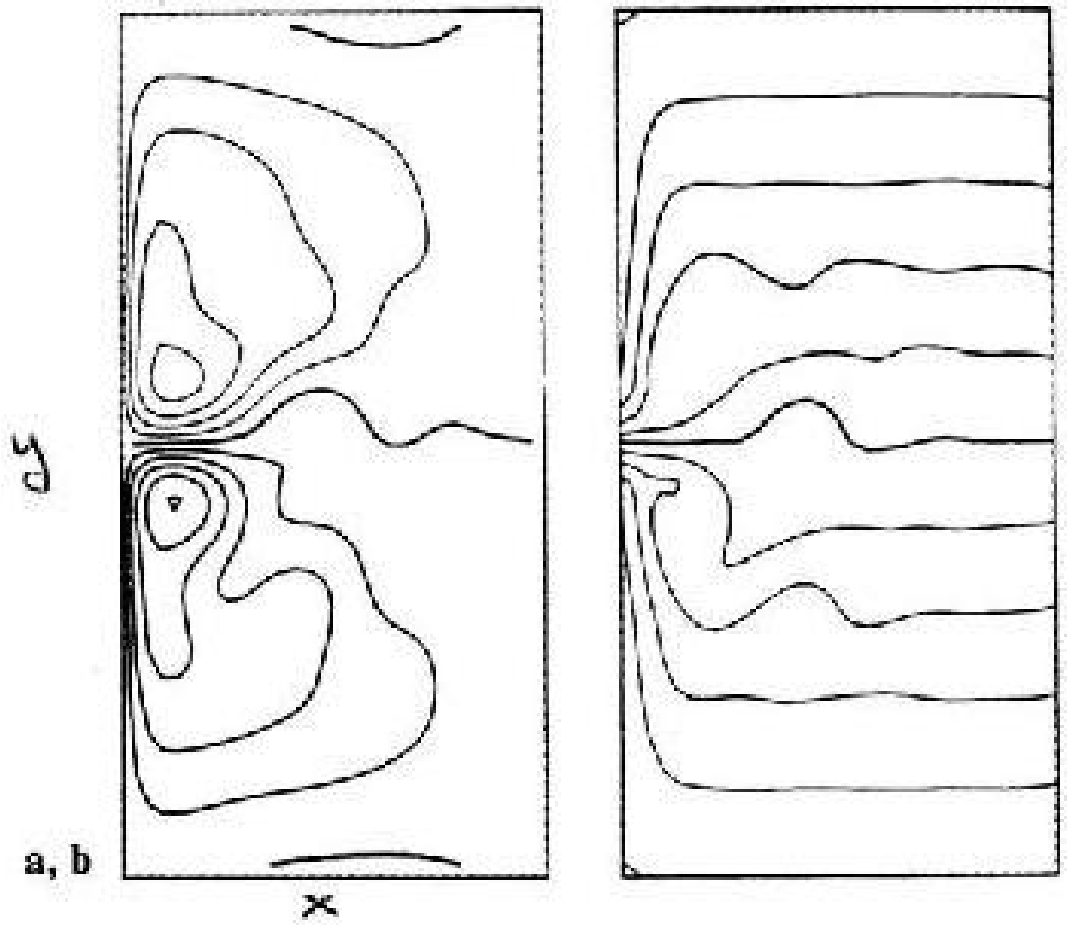

Time-averaged $\overline{\psi}$ (left) and $\overline{Q}_{qg} = \overline{\zeta} + \beta y$, $\zeta = \nabla_h^2 \psi$ (right) from a nonlinear, QG, barotropic model with a steady, "double gyre" wind stress (*i.e.*, $\tau^{s\,x}(y)$ is maximum in the center) (Marshall, 1984). The averaged circulation is unstable, mesoscale eddies arise, and the eddy potential vorticity flux divergence $\overline{\mathbf{u}_g' \cdot \nabla Q_{qg}'} = \overline{J[\psi', Q_{qg}']} \neq 0$ allows $\overline{\psi} = \overline{\Psi}/h$ to be larger than the Sverdrup flow in the interior recirculation gyres around the WBC separation site. The model's potential vorticity equation with both bottom drag and horizontal eddy viscosity is

$$\partial_t Q_{qg} + J[\psi, Q_{qg}] = -\frac{1}{\rho_0 h}\frac{\partial \tau^{s\,x}}{\partial y} - \frac{R}{h}\nabla^2\psi - \nu_4 \nabla^6 \psi \,.$$

$J[a,b] = \partial_x a \partial_y b - \partial_y a \partial_x b$ is the Jacobian operator.

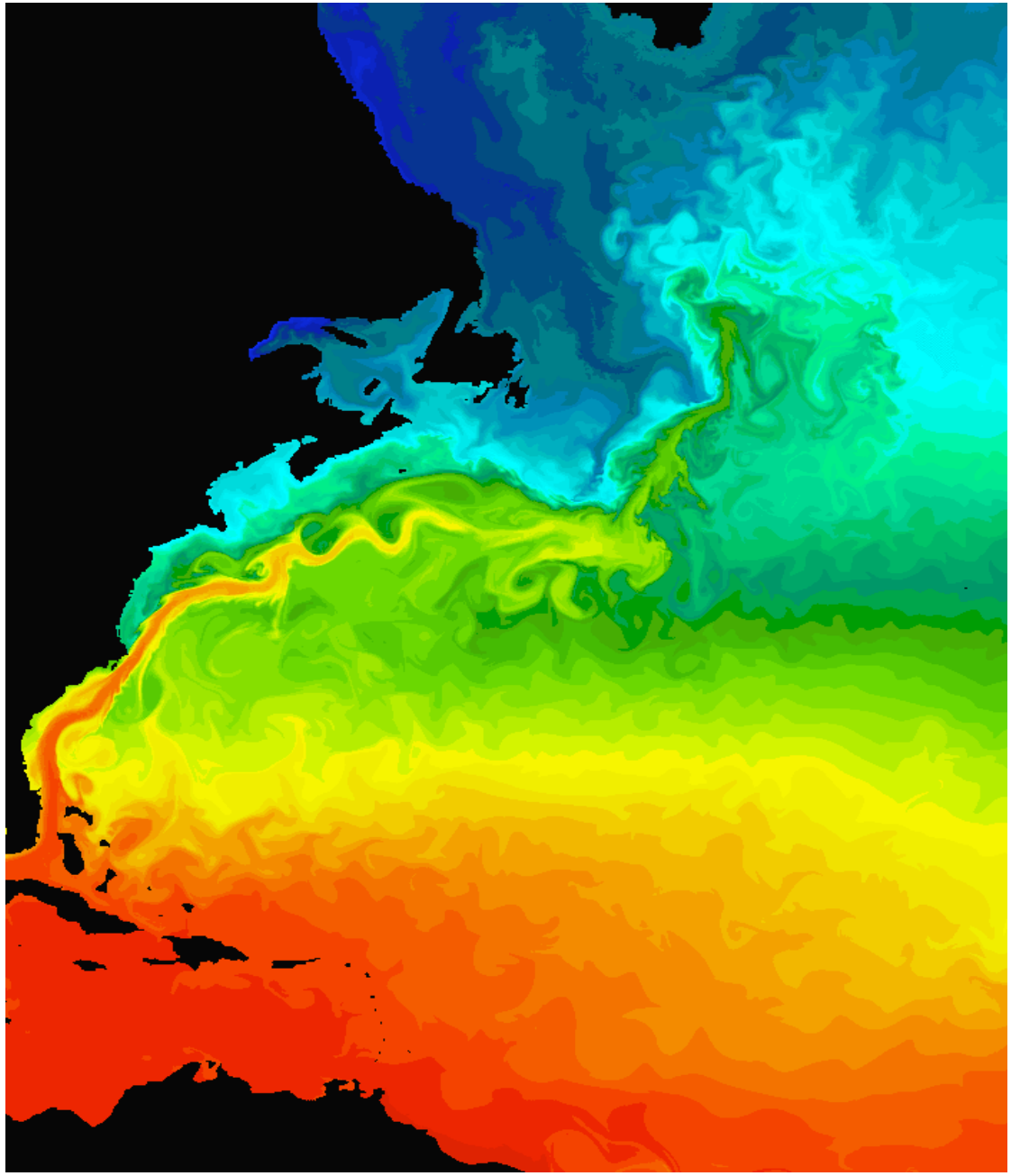

Instantaneous of SST in Western North Atlantic. Notice the warm, narrow, separated Gulf Stream (subtropical WBC), ubiquitous mesoscale eddies, southward cold Labrador Current (subpolar WBC), and cold St. Laurence river outflow. This figure is repeated.

Eddies near the Gulf Stream

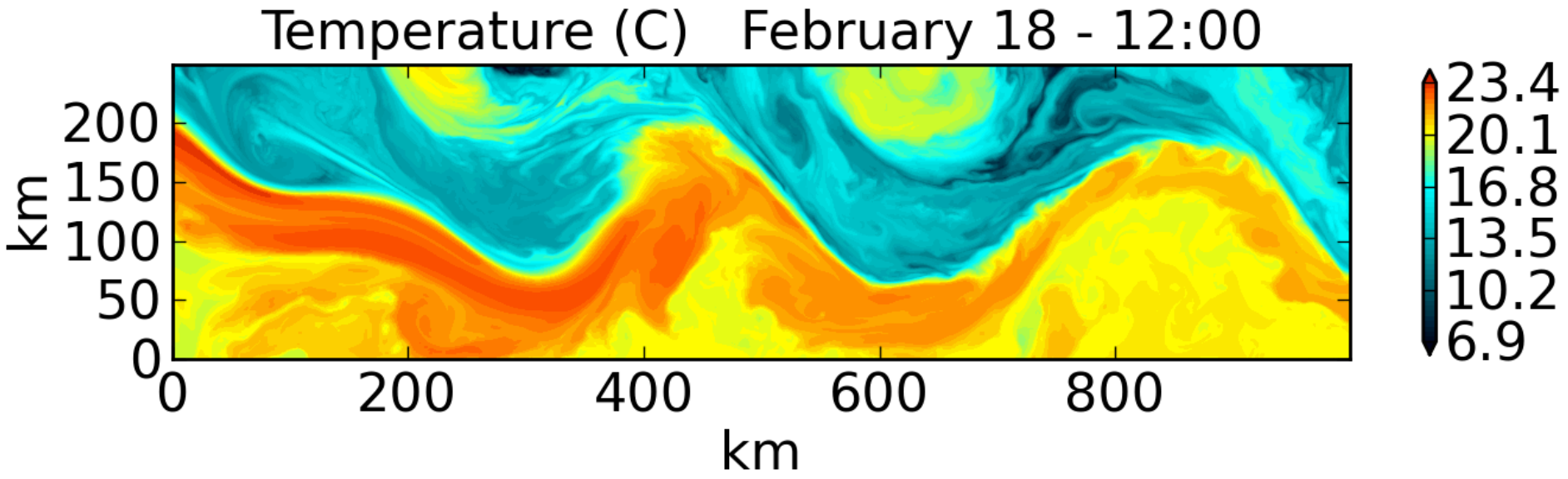

Instantaneous SST along a Gulf Stream sector downstream of its separation from the western boundary. The main flow is from left to right along the contours of strong temperature differences. Notice the large mesoscale meanders and alternating regions of a sharp, smooth North Wall on the downstream meander faces; submesoscale instability wiggles on the upstream faces; and backward streamers off the top of the central crest. To the north are two warm-core, anticyclonic Gulf Stream Rings that formed earlier by pinching off large meander crests. (From a numerical simulation in our research group.)

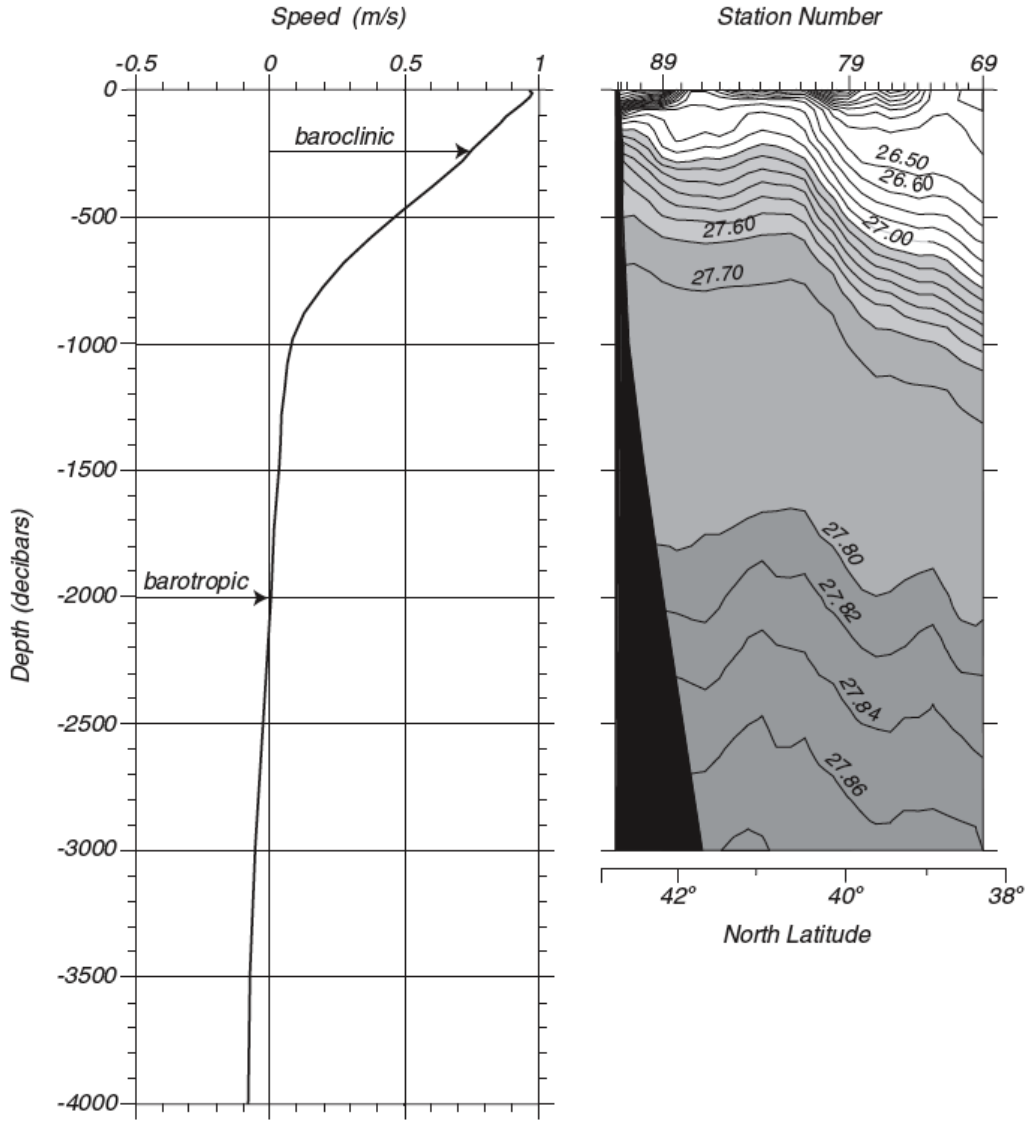

Meridional section of density ($\sigma = (\rho - 10^3)$ kg m^{-3}) from hydrographic stations taken across the Gulf Stream downstream from its point of separation from the western boundary (right) and the vertical profile of the geostrophic zonal current [m s^{-1}] at its center (left), integrated from thermal wind with a "level of no notion" at z = - 2000 m. The gyre circulation is mostly baroclinic, with the strong currents in and above the main pycnocline; the mean flow at 2000 m should be added to have the total flow. (Stewart, 2008)

Upper-Ocean Flow Structure: Compensating Surface and Pycnocline Slopes

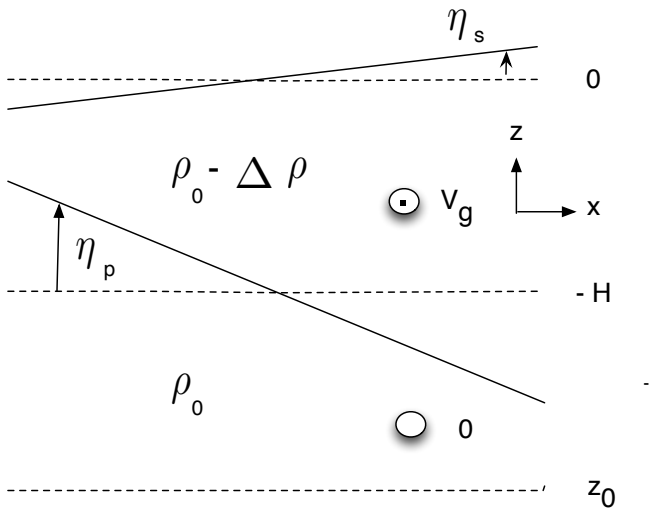

$$\partial_z p = -g\rho \;\Rightarrow\; p(z) = p_o + g\int_z^\eta \rho(z')\,dz'$$

For $z_0 < -H + \eta_p$,

$$p(z_0) = p_0 + g(\rho_0 - \Delta\rho)\,(\eta_s + H - \eta_p) + g\rho_0(-H + \eta_p - z_0)$$

$$\Rightarrow\; \partial_x p(z_0) = g(\rho_o - \Delta\rho)\,\partial_x\eta_s + g\Delta\rho\,\partial_x\eta_p$$

Therefore, there is no horizontal pressure gradient below the pycnocline if

$$\partial_x\eta_p = -\frac{\rho_0 - \Delta\rho}{\Delta\rho}\,\partial_x\eta_s \approx -\frac{\rho_0}{\Delta\rho}\,\partial_x\eta_s\,.$$

This is consistent with no deep flow and an upper-layer geostrophic flow of

$$v_g = \frac{g}{f}\,\partial_x\eta_s\,.$$

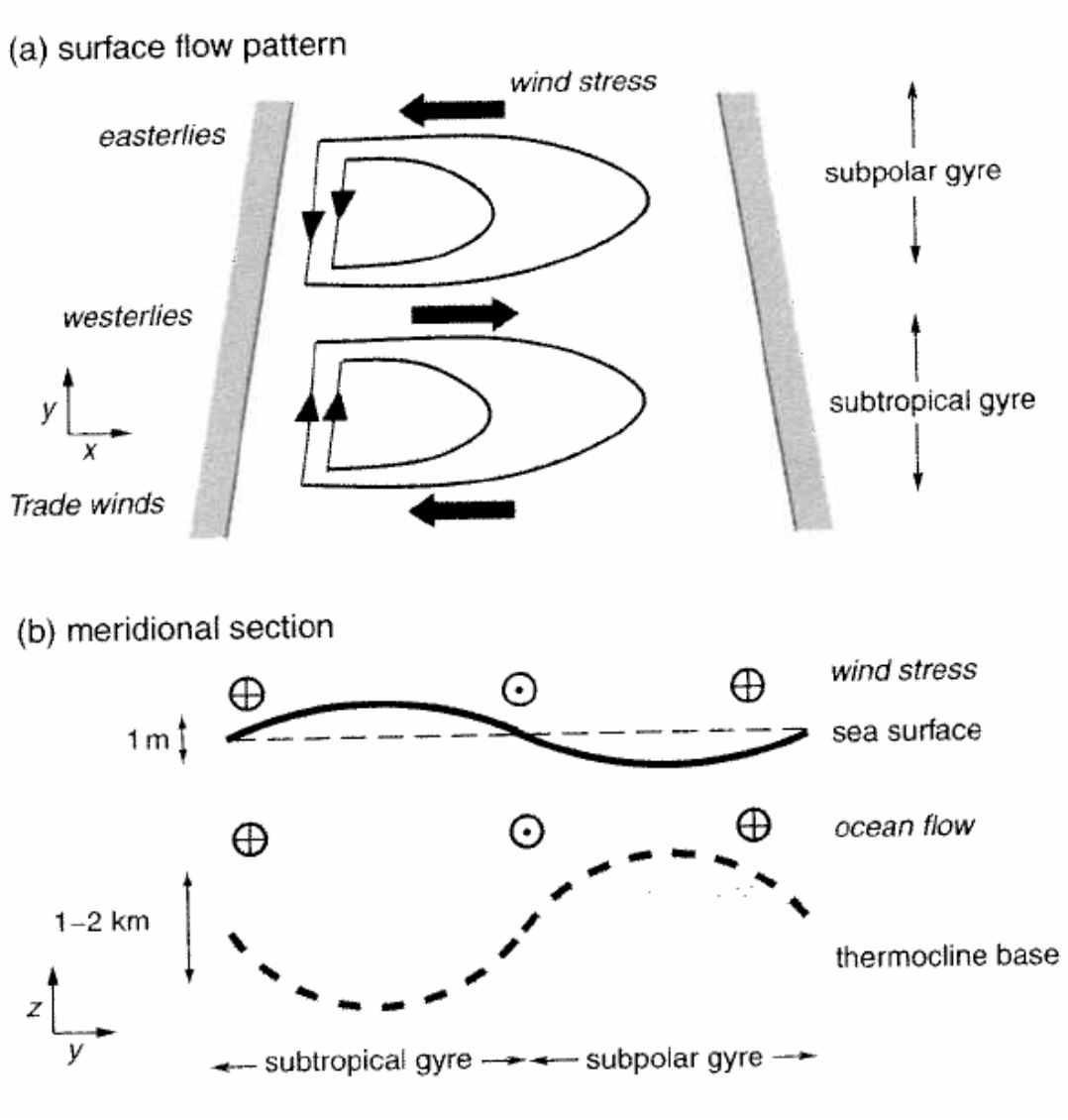

A cartoon of the 3D structure of subtropical and subpolar gyres in the northern hemisphere. The pycncline depth h_{pyc} mirrors the surface elevation η because of the surface intensification of the geostrophic gyre flow. (Williams and Follows, Fig. 8.1; $n.b.$, the depth range for h_{pyc} is several 100 m, not 1-2 km.)

2. Pycnocline Stratification and Ventilation

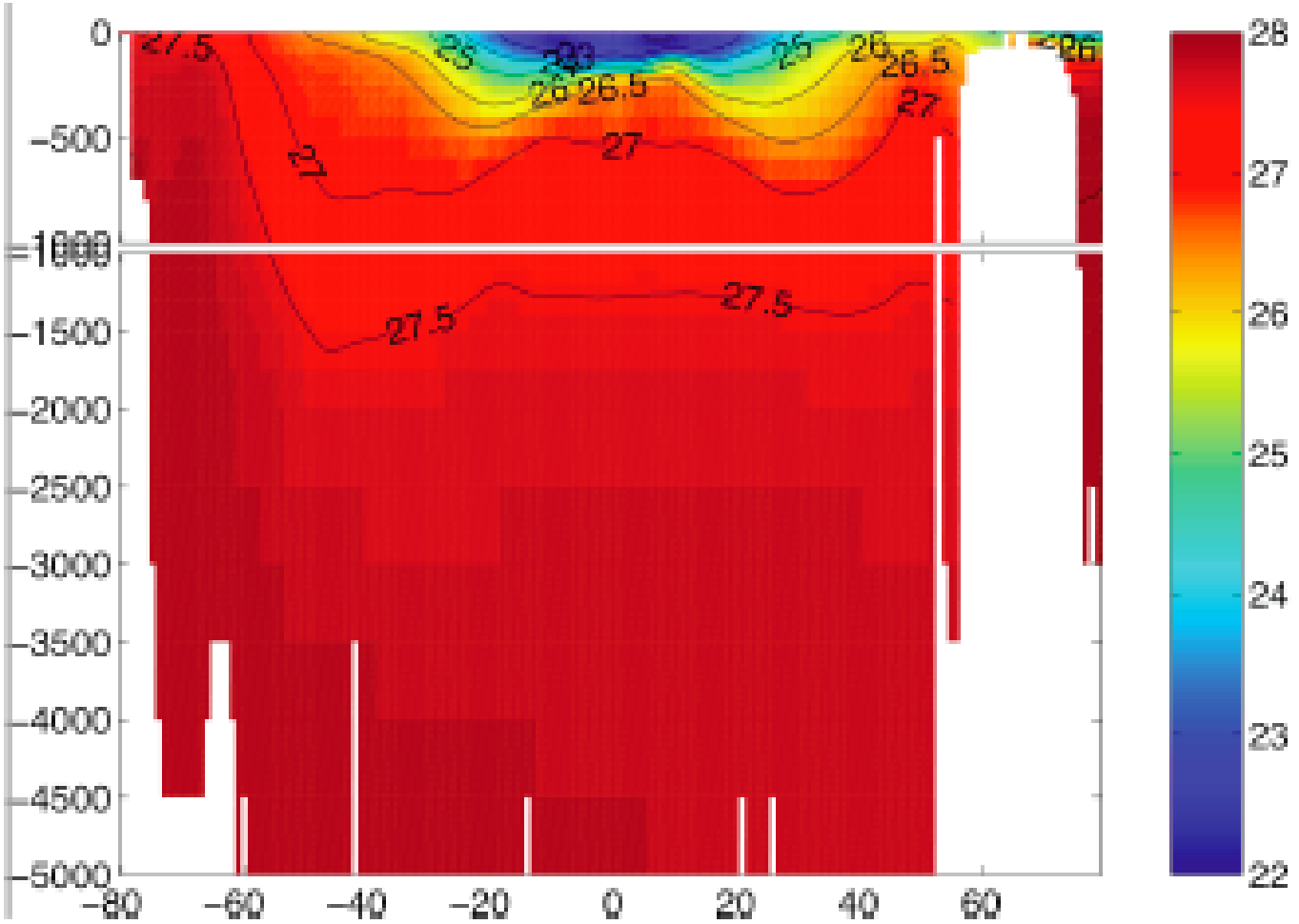

Meridional section of potential density referenced to the surface pressure p_0 (*i.e.*, $\sigma_0 = (\rho(p_0) - 10^3)$ [kg m^{-3}]) along 170 W in the Pacific (Garcia *et al.*, 2005). Potential density is evaluated by adiabatic displacement to a common reference pressure, which removes the effect of compressibility.

What sets the spatial pattern of the pycnocline? Mostly ventilation at "outcrops" (intersections of an isopycnal surface with the top surface) and advection/eddy-diffusion along isopycnals as the descend into the interior.

Estimates of the Subtropical Pycnocline Depth

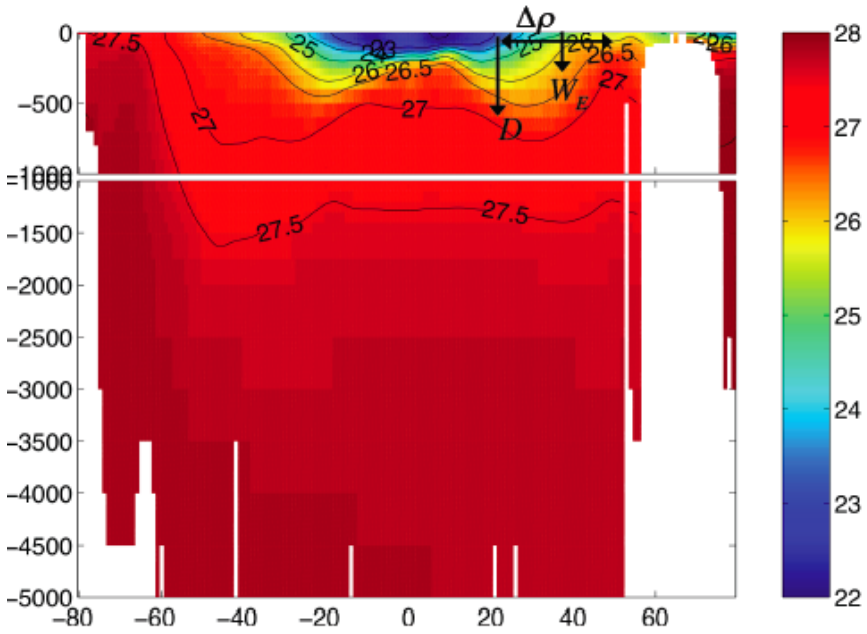

$L \approx 5 \times 10^6$ m
$f \approx 10^{-4}$ s^{-1}
$\beta \approx 2 \times 10^{-11}$ m^{-1} s^{-1}
$\Delta b = g\Delta\rho/\rho_0 \approx 0.02$ m s^{-2}
$W_{ek} \approx 2 \times 10^{-6}$ m s^{-1} (slide 2)

Assume planetary geostrophic thermal wind and vorticity balances and do scale estimation:

$$f\partial_z v = \partial_x b\,, \quad \beta v = f\partial_z w \quad \Rightarrow \quad D \sim \left(\frac{W f^2 L}{\beta \Delta b}\right)^{1/2}\,.$$

If W is from vertical buoyancy advection-diffusion balance with small $\kappa_v \approx 10^{-5}$ m^2 s^{-1} as measured,

$$w\partial_z b = \kappa_v \partial_{zz} b \quad \Rightarrow \quad W_{dif} \sim \frac{\kappa_v}{D}\,, \quad D_{dif} \sim \left(\frac{\kappa_v f^2 L}{\beta \Delta b}\right)^{1/3} \approx 100\,m\,,$$

which is smaller than observed. But if $W = W_{ek}$ is from Ekman pumping, $D_{ek} \approx 500$ m, which is roughly what is observed in subtropical gyres.

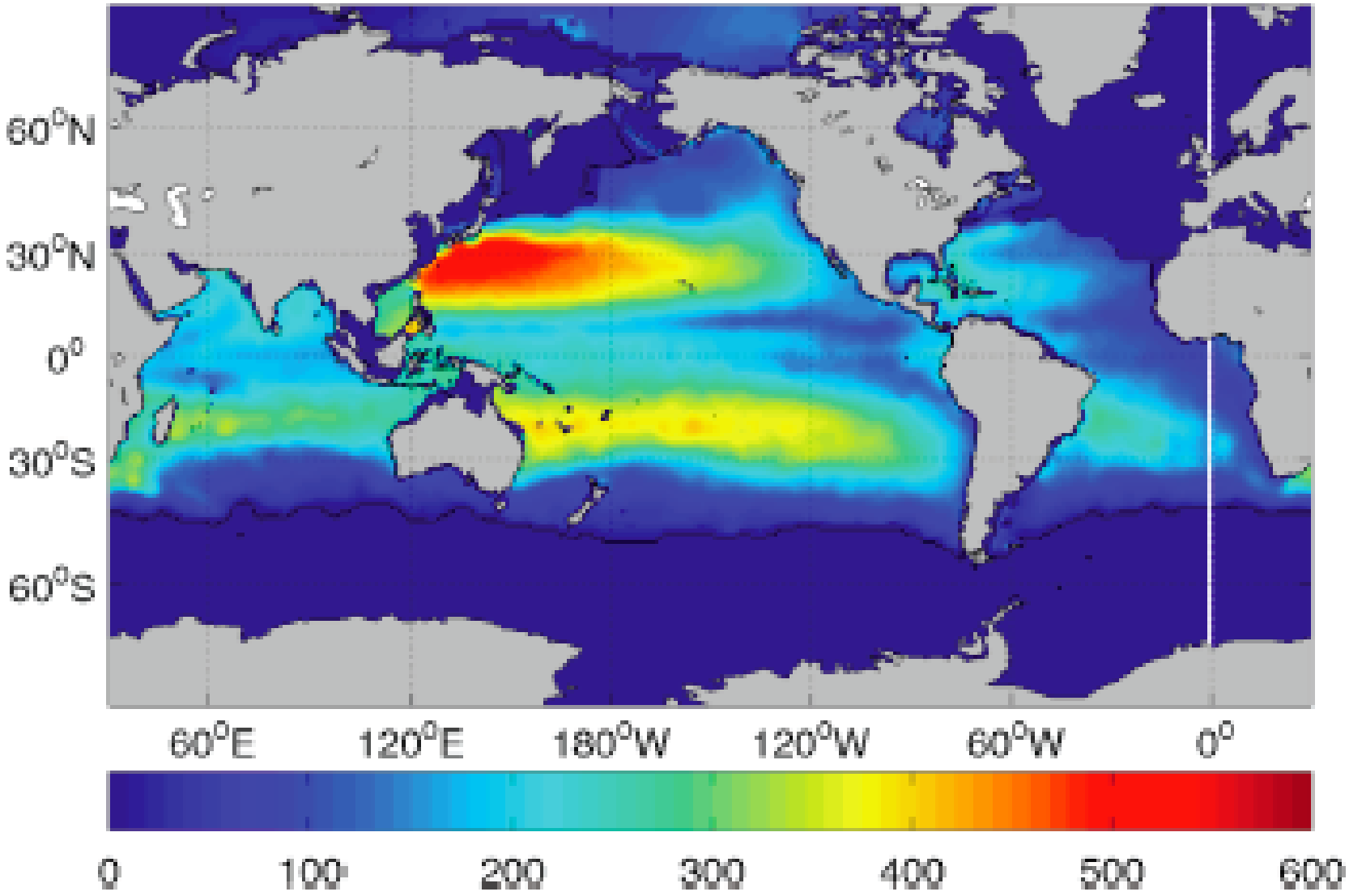

Depth [m] of the isopycnal surface $\sigma_0 = 26.2$ kg m^{-3} in winter (Garcia *et al.*, 2005). The intersection with the mixed layer or surface (black line) is the outcrop. Thus, the upper subtropical pycnocline density surface is "formed" by ventilation around 40^o N and S.

Subduction in a Subtropical Gyre

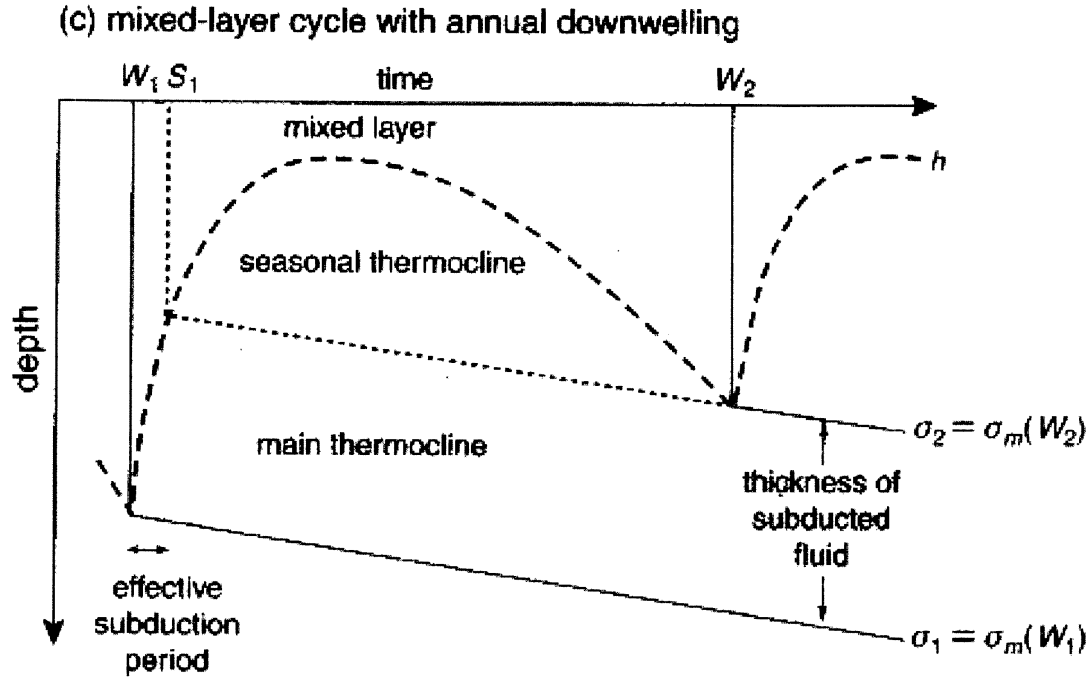

A sketch of the annual cycle of the mixed layer following the movement of the water column moving southward in a subtropical gyre where there is also downward Ekman pumping. Fluid is permanently subducted into the main thermocline during a short period after the end of winter W_1 until S_1. Outside this period ($i.e.$, from S_1 until the end of the next winter W_2), fluid is transfered from the mixed layer into the seasonal thermocline, and then re-entrained into the mixed layer during the following autumn and winter. (WF, Fig. 10.10)

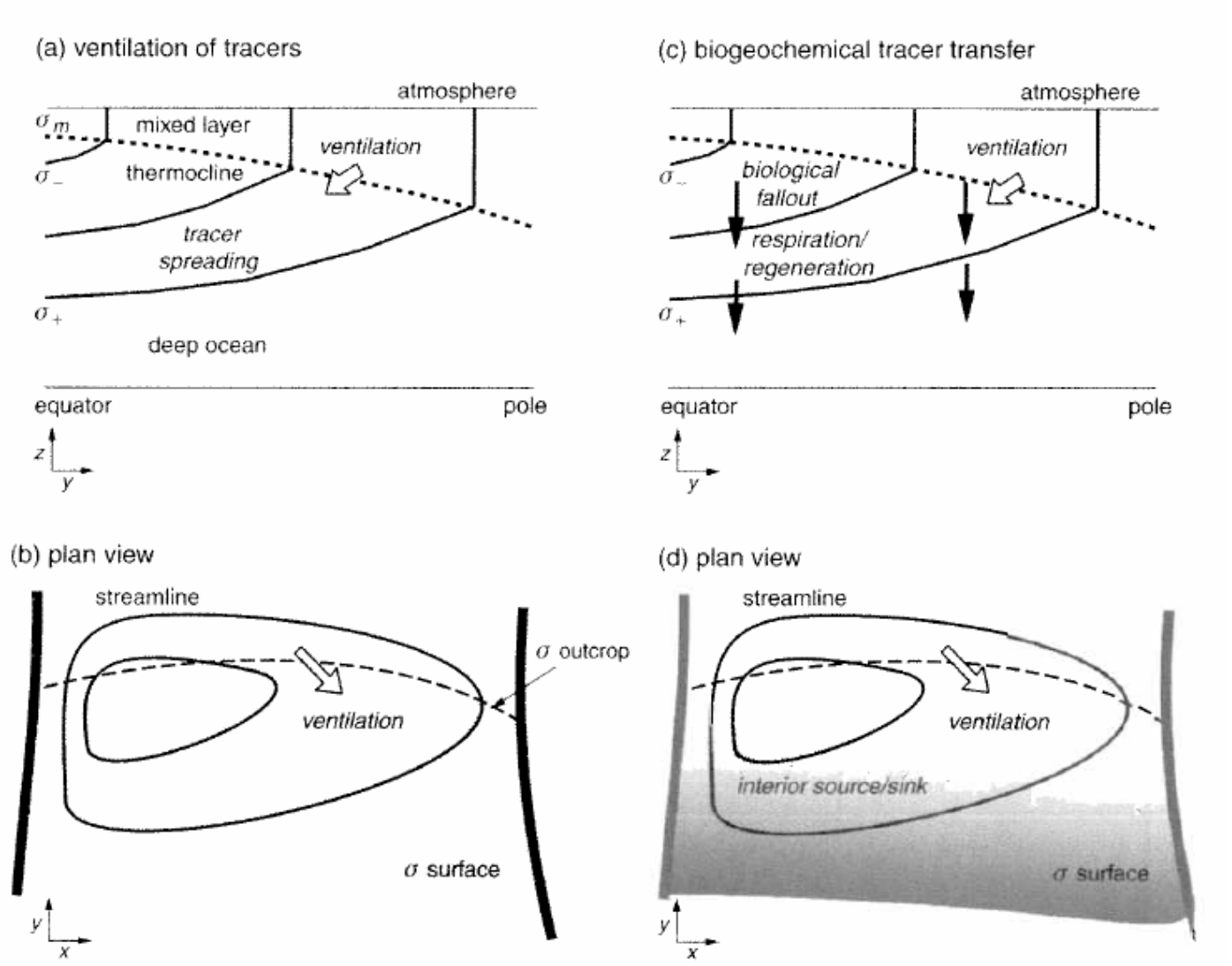

Another sketch of ventilation as it relates to passively advected and mixed tracers *vs.* biogeochemical materials with falling particulates. White arrows indicate transfer from the mixed layer to the stratified interior, and black arrows indicate detrital particle sinking and other biogeochemical transformations. The lower panel shows the relation between ventilation and subtropical gyre circulation. (WF, Fig. 10.2)

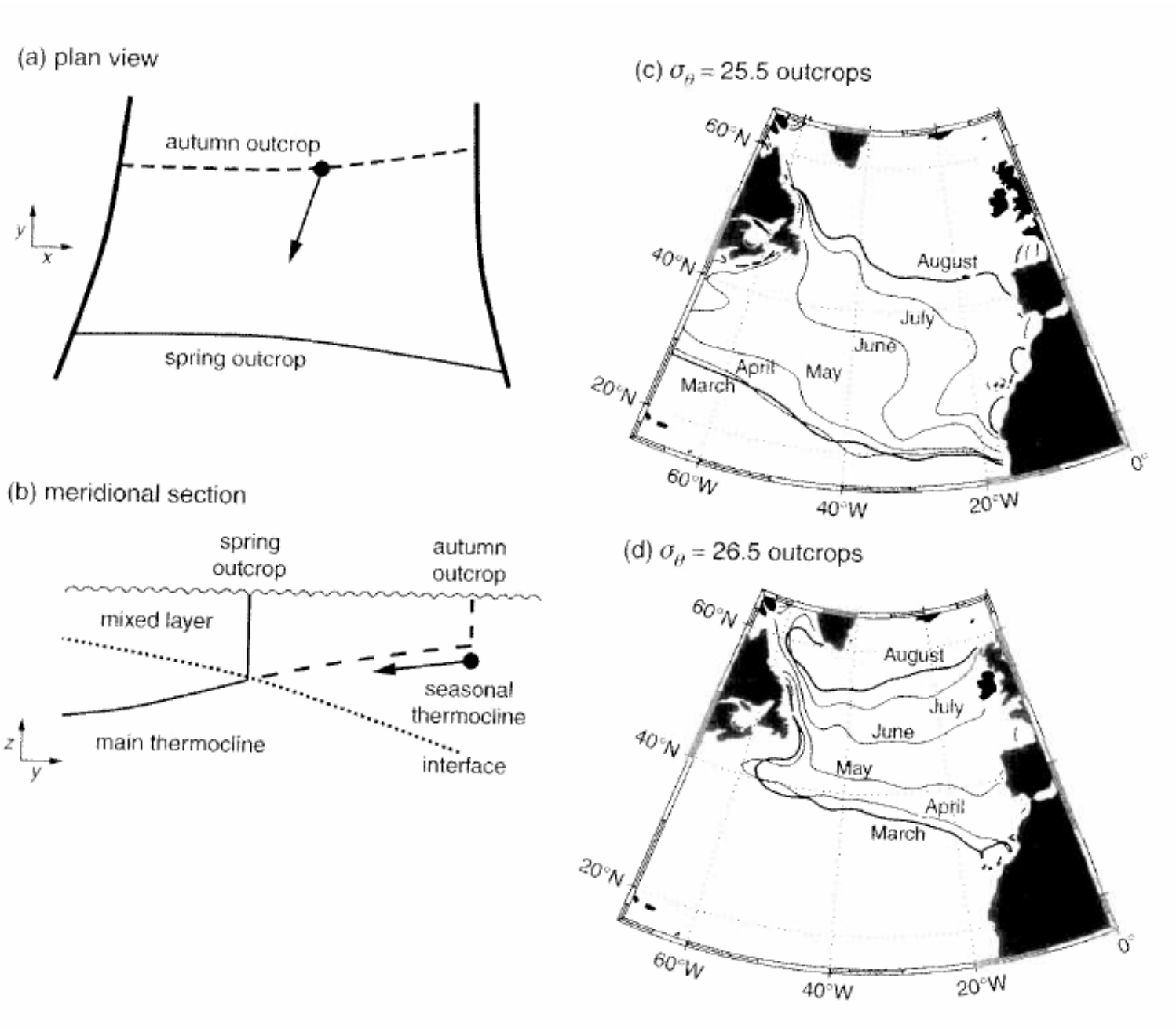

Pattern of seasonal variation of an isopycnal outcropping, and the mean location of the outcrop for $\sigma = 25.5$ in the North Atlantic. (WF, Fig. 10.11)

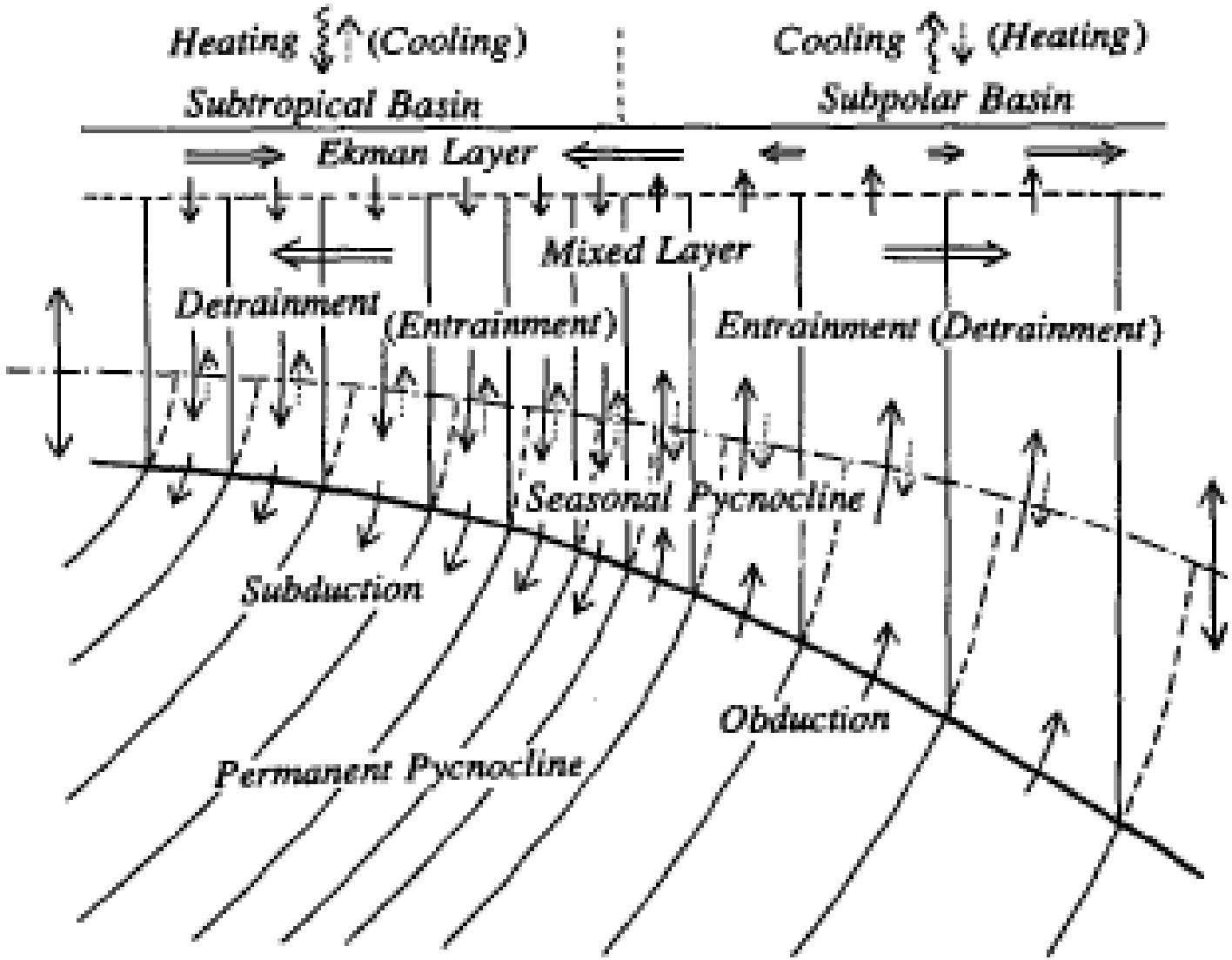

Sketch of the transformation of water from one density to another as a result of surface buoyancy flux and Ekman pumping. The net transformation of density is balanced by $subduction$ (down) or $obduction$ (up) of the water down into or out of the pycnocline, at a velocity $R = w + D\,h_{ML} \,/\, Dt$, relative to the changing mixed layer depth h_{ML}. (Qiu and Huang, 1995)

Transient Tracers of Ventilation

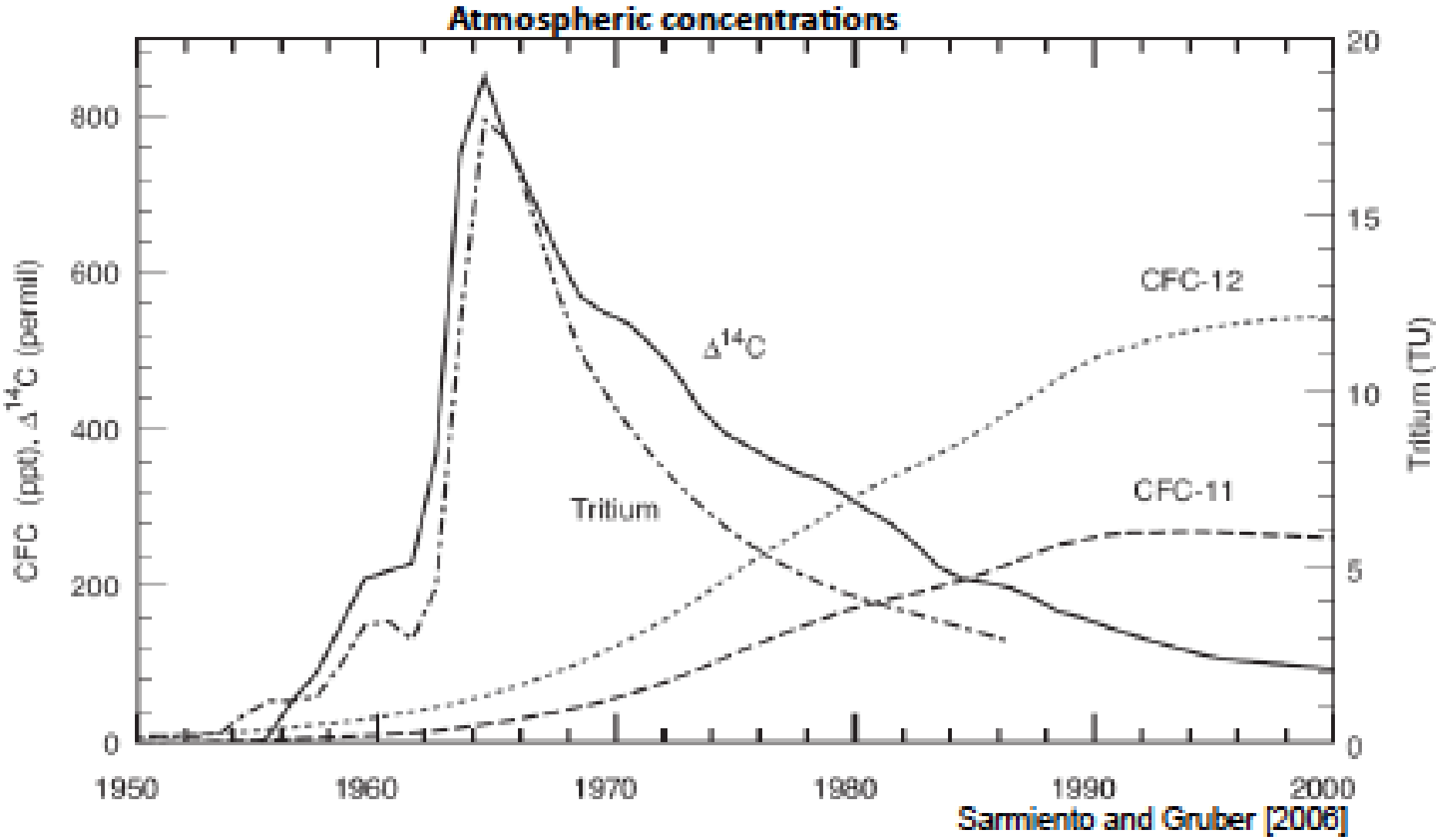

Atmospheric history of anthropogenic gases that have invaded the ocean on decadal time scales. The sources are atomic bombs (^{3}H and ^{14}C) and refrigerators (CFCs). Their evolving distributions in the ocean are used to infer rates of subduction and circulation patterns.

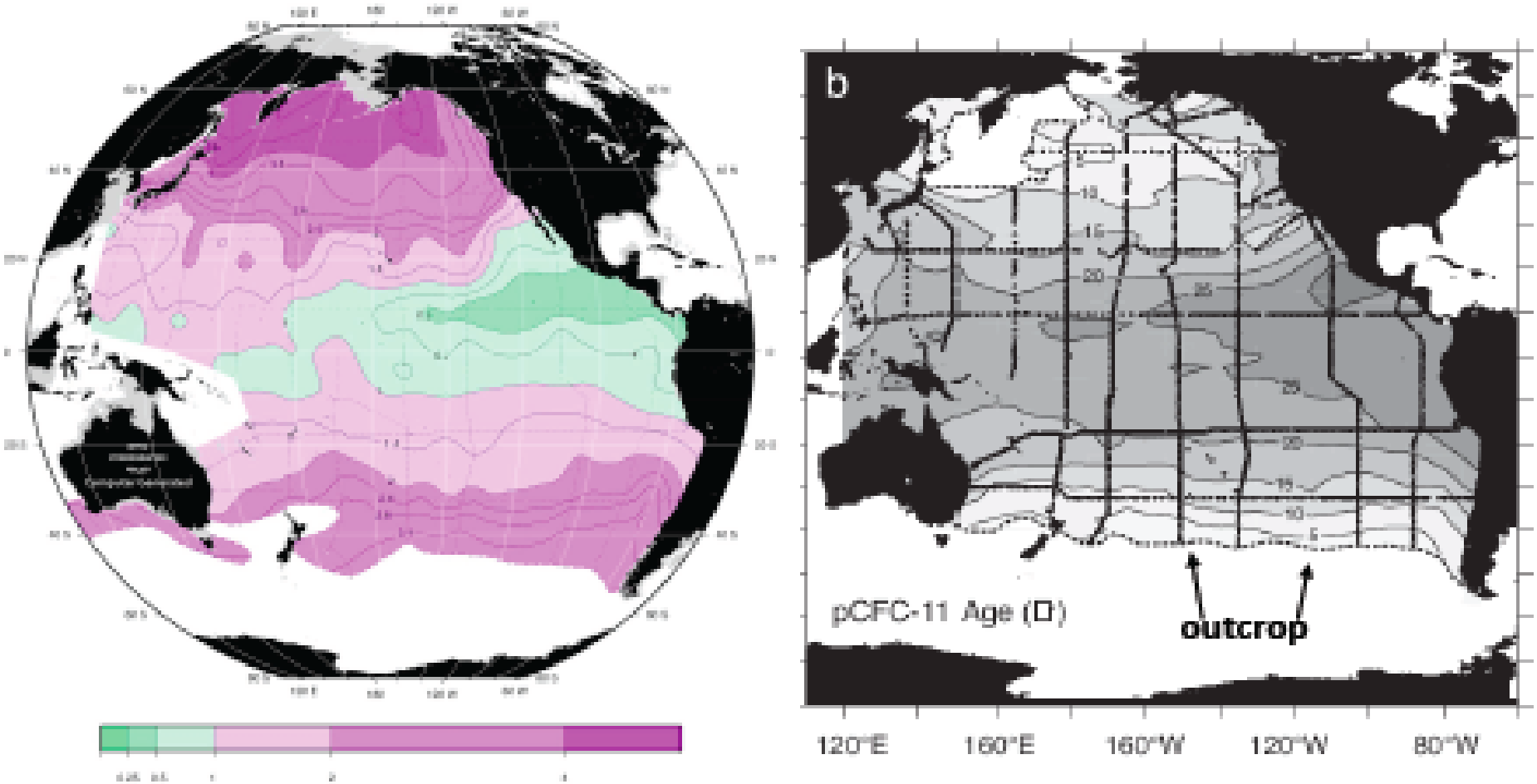

Thermocline ventilation indicated by the distribution of chloroflourocarbon (CFC-11) in concentrations (pmol m^{-3}, left) and indicated age (average years since atmospheric exposure)) and hydrographic station locations (right). These are mapped on the $\sigma_0 = 26.2$ and 26.4 kg m^{-3} surfaces in the pycnocline, respectively ($i.e.$, nearly the same). By matching the CFC partial pressure to the atmospheric history we define the "age" of the water since last contact with the atmosphere. Notice the shadow zone along the tropical eastern boundary where the water is especially old ($i.e.$, barely ventilated and "contaminated" by mixing with adjacent waters). (Sarmiento and Gruber, 2006)

3. Equatorial Currents

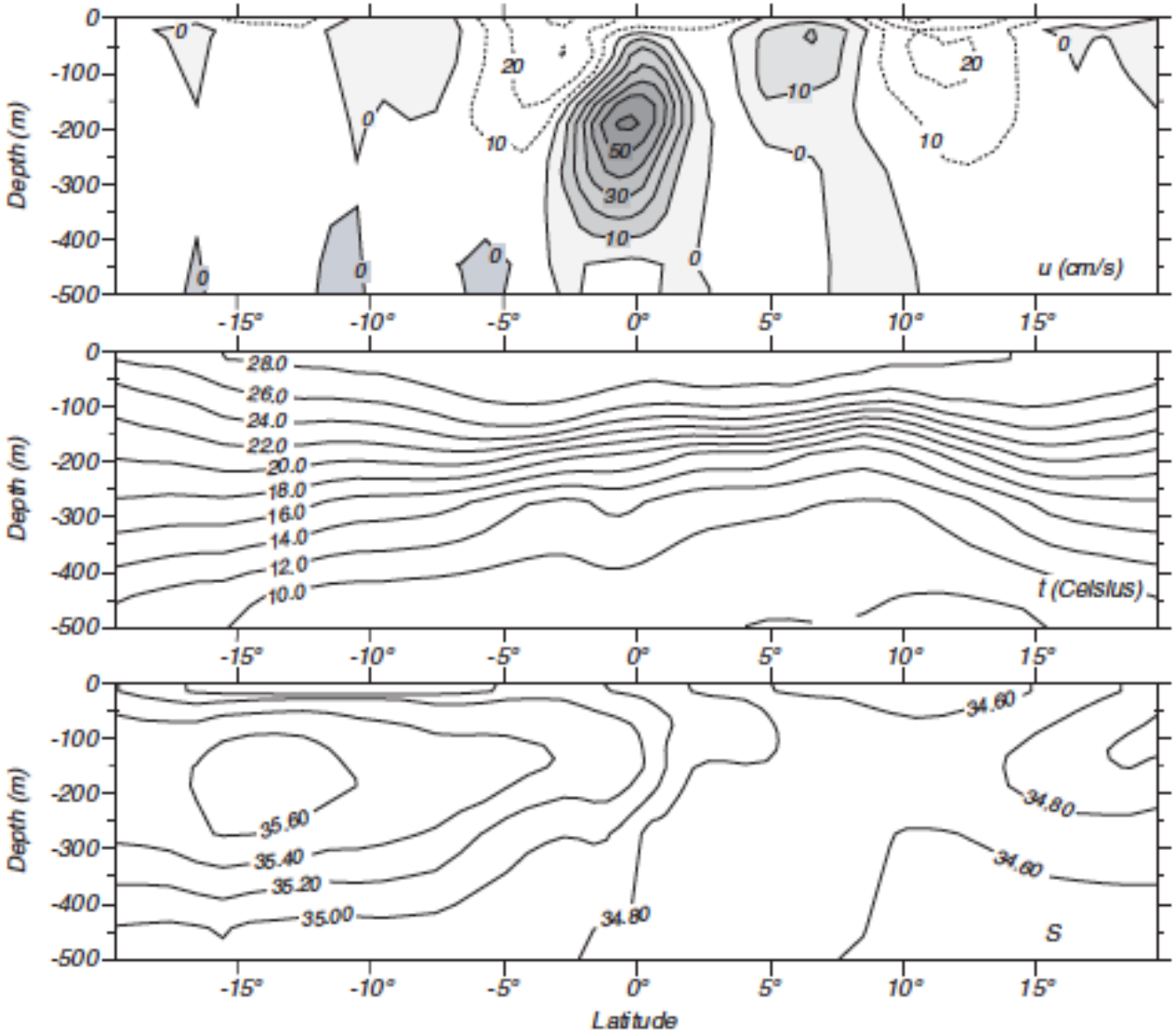

Meridional section in the central Pacific: zonal velocity u [cm s^{-1}], T [C], and S [PSU]. Notice the Equatorial Undercurrent, North Equatorial Countercurrent (9N), and westward zonal currents. T is the main influence on stratification & geostrophic balance for the currents, and S has an inter-hemispheric water mass boundary. (From an OGCM with data assimilation; Stewart, 2008.)

Equatorial Zonal Section

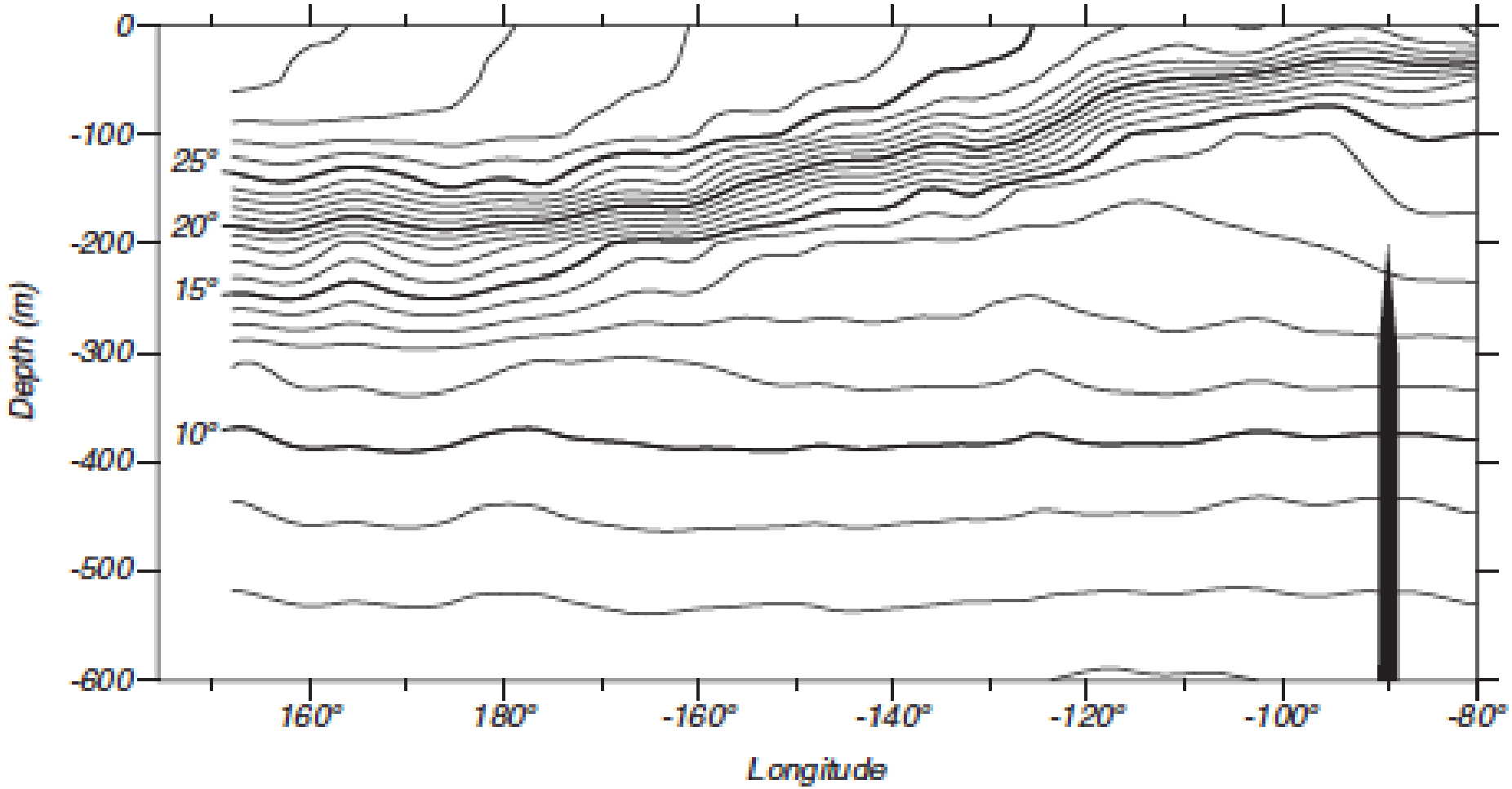

The mean, upper-ocean, thermal structure in a zonal section along the equator in the Pacific from north of New Guinea to Ecuador. The upward tilt of the thermocline indicates the westward surface current, eastward Undercurrent, and eastern upwelling. This tilt oscillates during an El Niño event with associated changes in SST and zonal wind stress. (Stewart, 2008)

Mean Dynamical Balance at the Equator

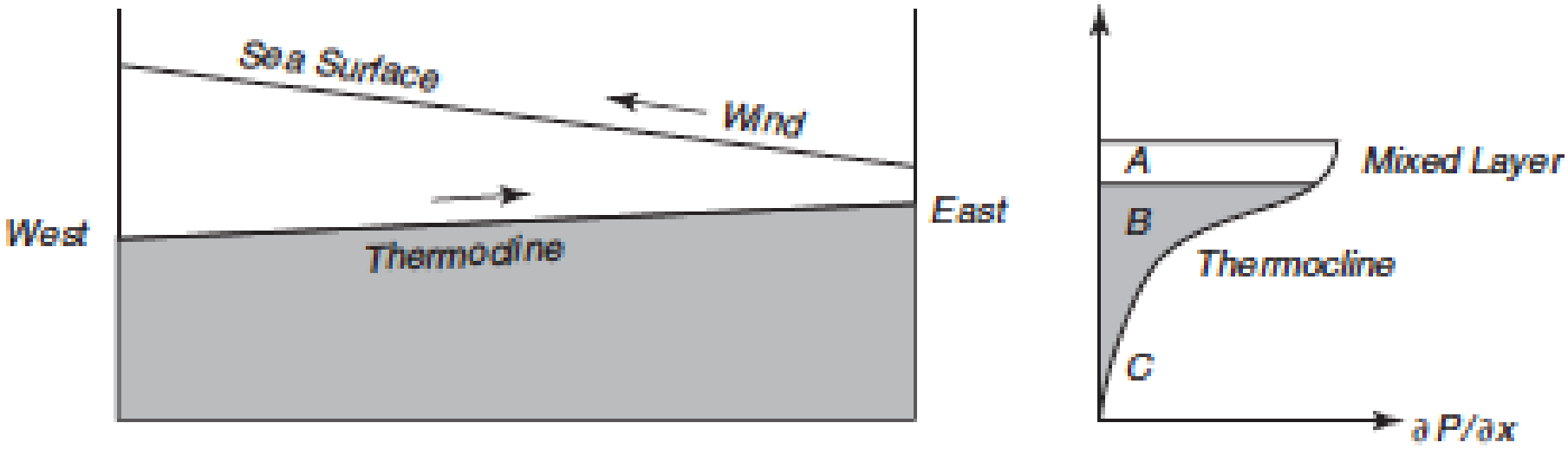

Left: Sketch of a zonal section of the thermocline and sea-surface topography along the equator. Right: Eastward pressure gradient ($\times -1$) in the central Pacific caused by the density structure at left. Wind drags surface water to the west creating a surface mound in the west. Below the turbulent boundary layer and in the thermocline, the associated pressure gradient force pushes the Undercurrent to the east. Coriolis force does not act to accelerate these zonal currents at the equator, but it does act in the meridonal momentum balance, $\beta y\, u \approx -\partial_y P$. (Stewart, 2008)

The opposing tilts of the surface and thermocline indicate confinement of the dynamic pressure signal to the upper ocean; $i.e.$, in the abyss the hydrostatic weight of the overlying water is approximately horizontally uniform. Opposing tilts are common for wind-driven currents (but not the ACC which extends much deeper).

4. Antarctic Circumpolar Current (ACC)

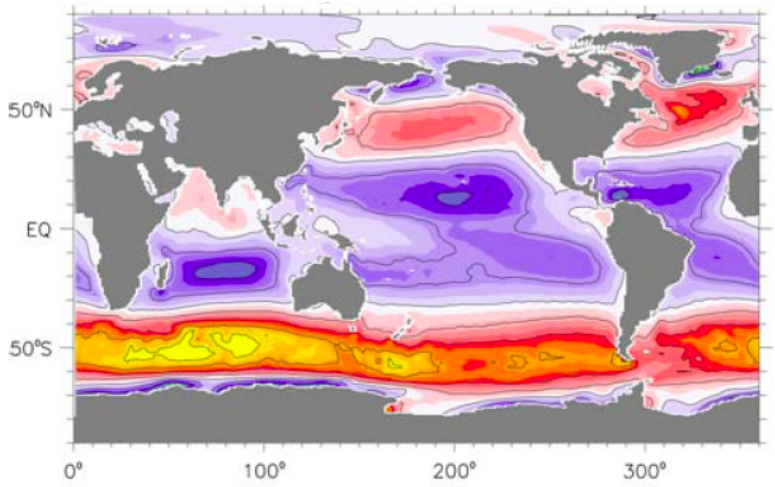

Mean zonal wind stress, colored at 0.02 N m^{-2} intervals. Notice strong eastward wind in the ACC. The waves are also large there, but Q and $\mathcal{F}$ are relatively small.

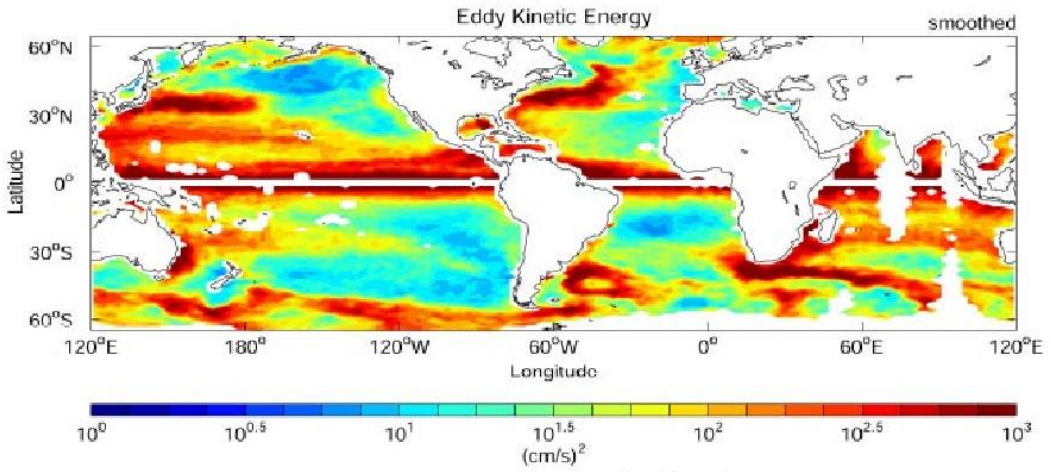

Mean surface eddy kinetic energy [cm^2 s^{-2}], large in the ACC. Both figures are repeated.

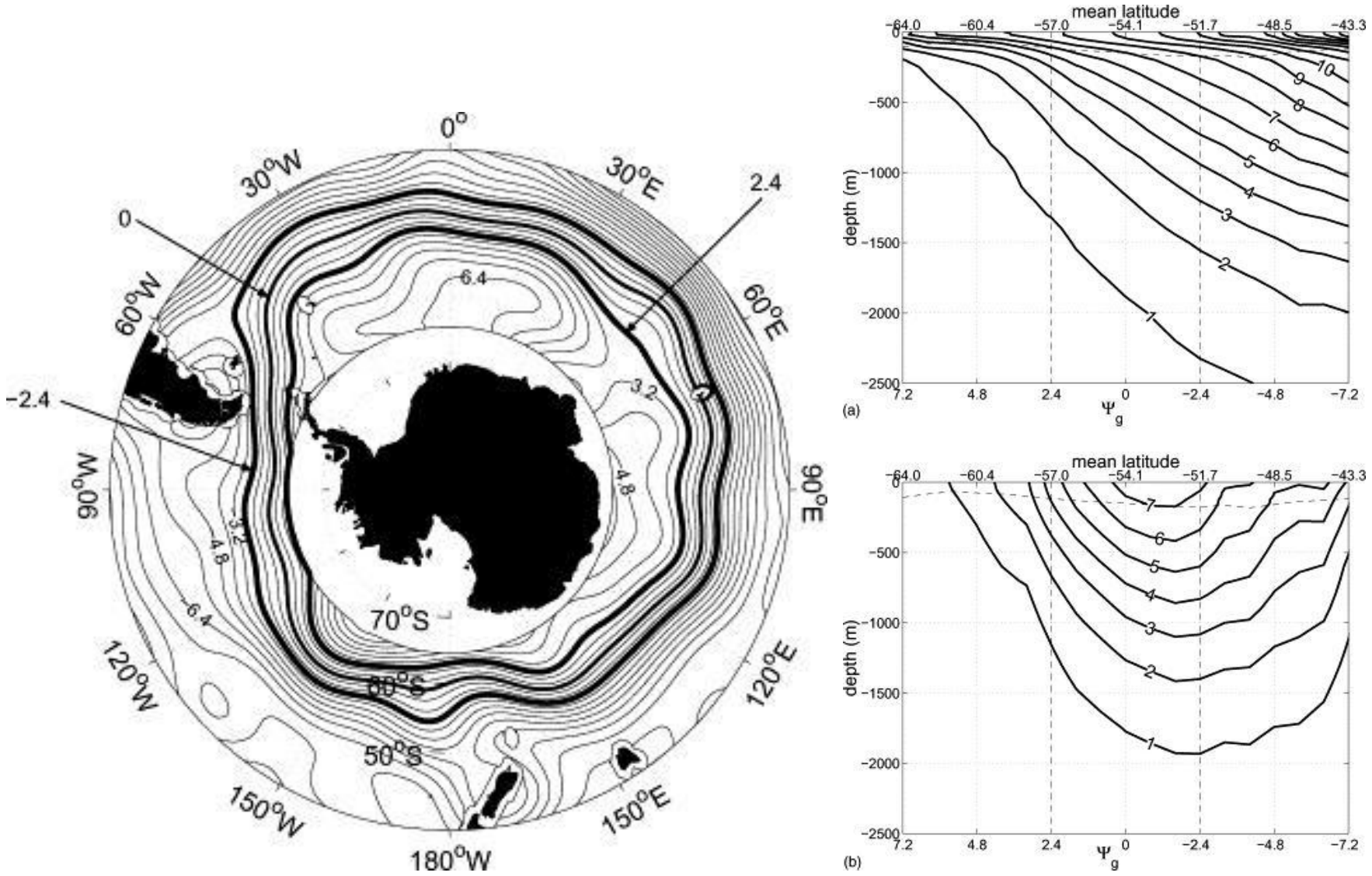

(Left) Mean surface geostrophic streamfunction, $\psi_g = g\eta/f$ in the ACC; the flow is mostly eastward but there are "standing eddy" meanders related to flow around topography. (Right) Zonally-averaged T [C] and u_g [cm s^{-1}] (assuming an abyssal level of no motion for the vertical integration of thermal wind balance) plotted against ψ_g in lieu of latitude; the ACC reaches deeper than wind gyres and equatorial currents. The total eastward transport is $>$ 100 Sv. (Karsten and Marshall, 2002)

Eddy-Mean Dynamics in the ACC

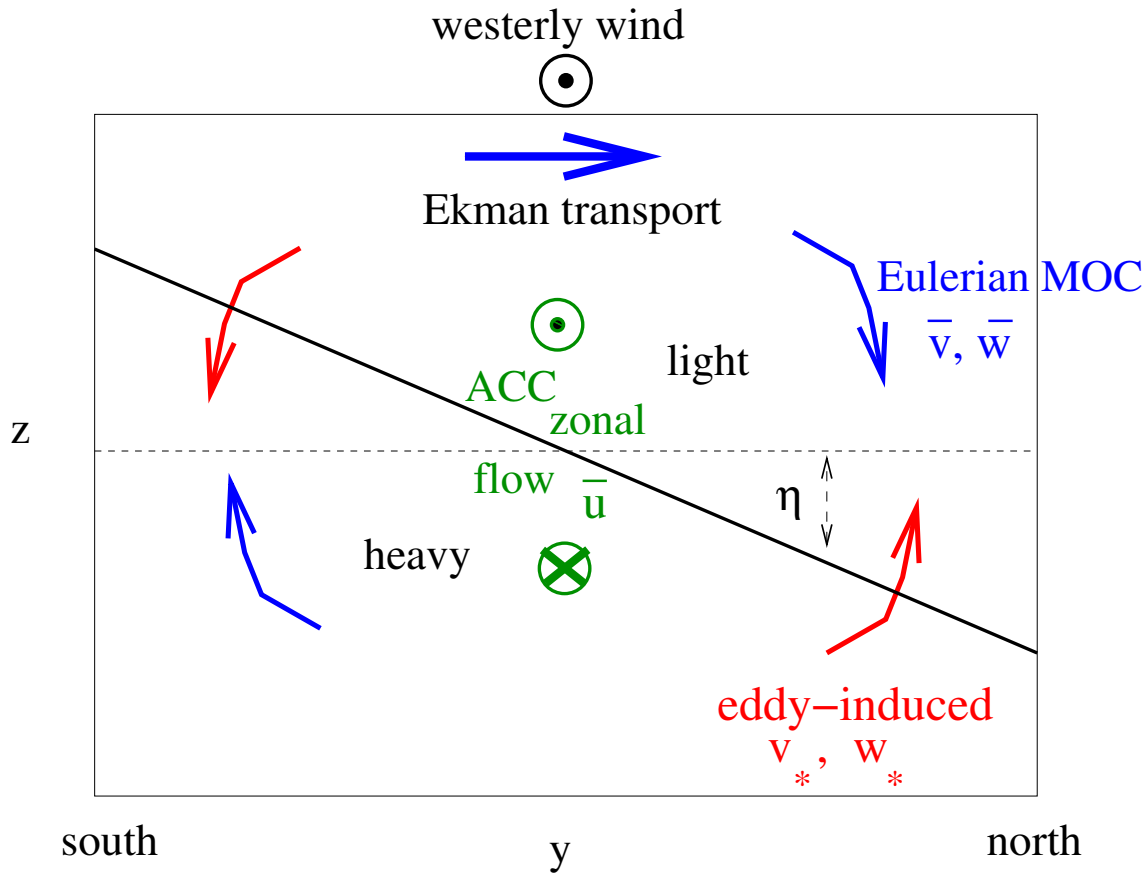

- mean wind in ACC: $\tau^{s\,x} > 0$.
- mean geostrophic ACC $\overline{u}(z)$ and pycnocline vertical displacement ($\overline{\eta} = -\,\overline{b}/\partial_z \overline{b} = -\,\overline{b}/N^2$):

$$\frac{\partial \overline{u}}{\partial z} \;=\; \frac{N^2}{f}\frac{\partial \overline{\eta}}{\partial y} \;=\; -\,\frac{1}{f}\frac{\partial \overline{b}}{\partial y} \;>\; 0 \qquad \text{because } f < 0\,.$$

- mean northward Ekman flux and (Eulerian) MOC that returns the flow at depth within the ACC (a.k.a. the Deacon Cell), *i.e.*, $\overline{\Phi}(y,z) > 0$ where $\overline{v} = -\,\partial_z \overline{\Phi}$, $\overline{w} = \partial_y \overline{\Phi}$.

- Mesoscale baroclinic instability $\Rightarrow$ eddy fluxes: $\overline{v'b'} < 0$ (poleward buoyancy flux); $\overline{v'\eta'} > 0$ (pycnocline flattening and vertical $\overline{u}$ flux); and $\overline{w'b'} > 0$ (restratification).
- mean material balance by eddy-induced "advection" and "diffusion" (mainly isopycnal):

$$\partial_t \overline{C} + \overline{\mathbf{u}} \cdot \overline{C} \;=\; -\nabla \cdot \overline{\mathbf{u}' C'} \;=\; -\mathbf{u}_* \cdot \nabla \overline{C} + \mathcal{D}[\overline{C}]\,.$$

- eddy-induced velocity $\mathbf{u}_*$, hence Lagrangian mean (a.k.a. residual velocity), $\overline{\mathbf{u}}^L = \overline{\mathbf{u}} + \mathbf{u}_*$. $\mathbf{u}_* \longrightarrow$ an "adiabatic" parameterization in OGCMs (Gent and McWilliams, 1990):

$$(v_*, w_*) \;=\; (-\partial_z, \partial_y)\Phi_*\,, \quad \Phi_* \;=\; \frac{\overline{v'b'}}{N^2} \;=\; -\,\overline{v'\eta'} \;\longrightarrow\; -\,\frac{\kappa_e}{N^2}\frac{\partial \overline{b}}{\partial y} \quad < 0 \text{ in ACC}\,.$$

- (x,t)-mean buoyancy balance in equilibrium in the nearly adiabatic interior:

$$(\overline{\mathbf{u}} + \mathbf{u}_*) \cdot \nabla \overline{b} \;=\; 0 \qquad \Rightarrow \qquad \overline{\Phi} + \Phi_* \;\approx\; 0 \quad \text{in the ACC.}$$

  because $\mathcal{D}[b]$ is zero with isopycnally-oriented eddy mixing.
- A vertical integral of the (x,z,t)-mean zonal momentum balance $\longrightarrow$

$$\frac{d}{dt}\,\overline{T}^x \;=\; 0 \;\approx\; \frac{\tau^{s\,x}}{\rho_0} + \int_{-h}^{0} \partial_z[f\Phi_*]\,dz - \frac{\tau^{b\,x}}{\rho_0} \;=\; \frac{\tau^{s\,x} - \tau^{b\,x}}{\rho_0}\,,$$

  where $f\Phi_* = -f\overline{v'\eta'} > 0$ is the eddy form stress (averaged horizontal pressure force acting on a sloping material surface) acting on interior isopycnals to transfer mean momentum downward (with zero vertical integral of its vertical divergence), and the bottom stress $\tau^{b\,x}$ includes both turbulent drag and topographic form stress, $-f\overline{v'(-h)'} < 0$ at $z = -h$.
- The real residual circulation, $\overline{\Phi} + \Phi_*$, is not quite zero because of "diabatic" mixing, though much smaller than $\overline{\Phi}$. The ACC residual circulation is important for global water masses.

.

Concept: Eddies act to tilt isopycnal surfaces toward the horizontal.

An eddy-induced overturning circulation advectively acts to flatten an isopycnal surface whose vertical position is $z = Z_{iso}(x)$. This reduces the avaliable potential energy ($i.e.$, associated with horizontal buoyancy gradients) of the mean baroclinic circulation by converting it to eddy potential and kinetic energy by the process of baroclinic instability.

A parameterization formala for this is

$$\Phi_* \sim \kappa_{iso}\, \partial_x Z_{iso}\,,$$

where κ_{iso} is a "horizontal" eddy diffusivity $\sim 10^3$ m^2 s^{-1}, $i.e.$, not associated with diapycnal material flux across an isopycnal surface.

This eddy-mean interaction process is a generic one in the ocean for the generation of mesoscale eddies and the limitation of mean isopycnal slopes.

5. Meridional Overturning Circulation (MOC)

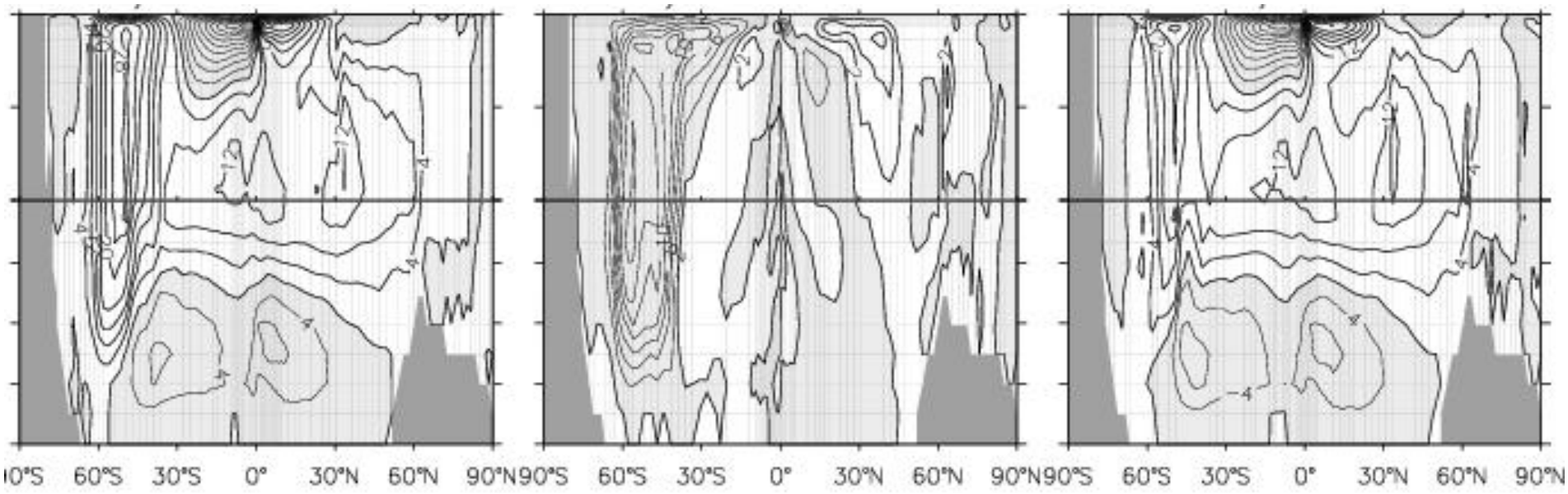

Meridional overturning streamfunction $\Phi(y, z)$ [Sv $= 10^6$ m^3 s^{-1}] for the global ocean from an OGCM. The depth scale is expanded in the upper 1km and compared to the abyssal layer below. The panels are (a) Eulerian-mean MOC (left), (b) eddy-induced MOC (center), and (c) their sum, the total Lagrangian MOC ($i.e.$, residual circulation; right). The contour intervals are 4 Sv in (a) and (c) and 2 Sv in (b). Notice the Deacon Cell and its partial eddy cancellation in the ACC, except near the surface where Q and $\mathcal{F}$ are diabatic. Away from the ACC the MOC is mostly comprised of either shallow Ekman cells or deep thermohaline ones. (From Gokhan Danabasoglu, NCAR)

.

Concept: There are shallow Subtropical Cells in the MOC that connect the Ekman pumping in the subtropical gyres and at the Equator.

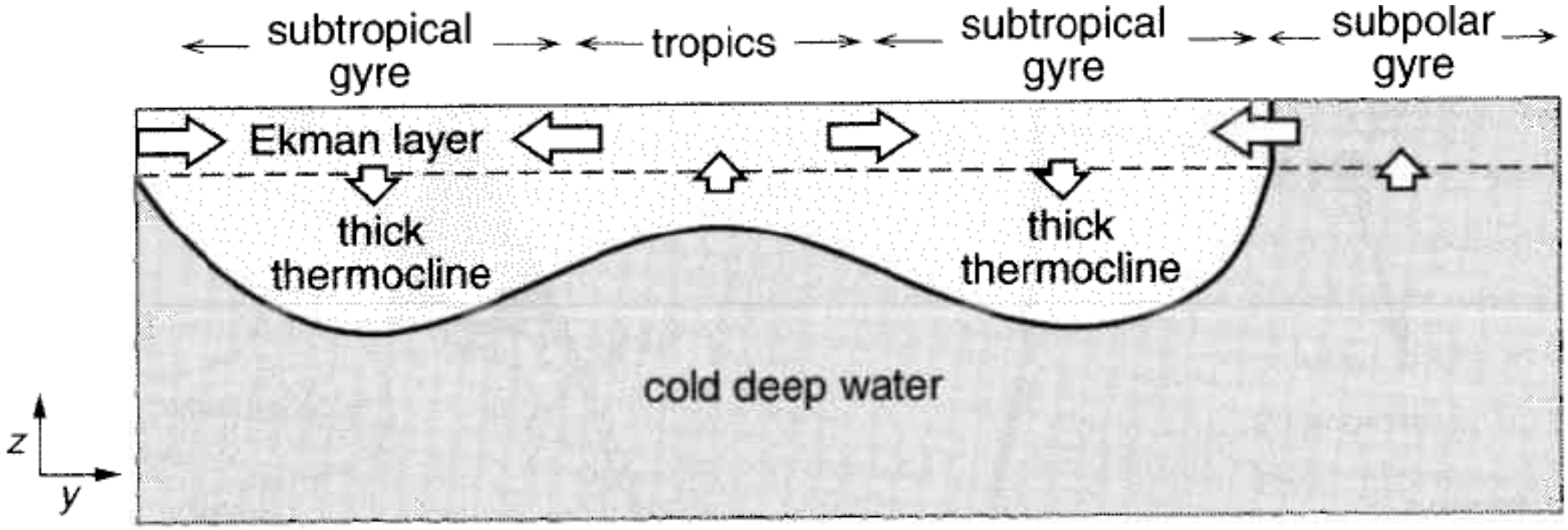

Schematic diagram of the Ekman pumping profile with latitude. The downwelling in the subtropical gyres connects to the upwelling near the Equator in shallow Subtropical Cells that close mainly within the pycnocline. (WF, Fig. 10.12)

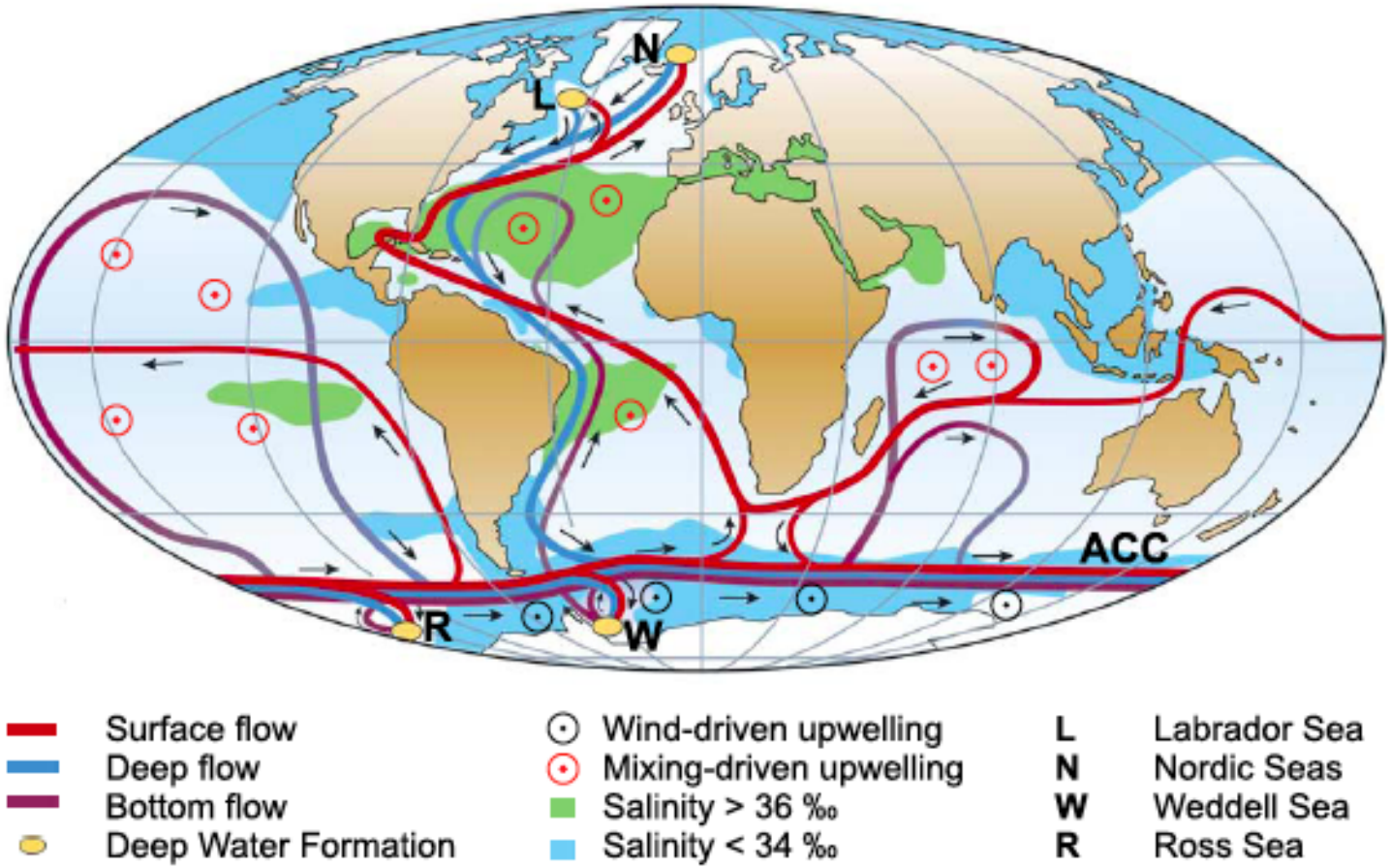

Sketch of the "observed" global overturning circulation system due primarily to thermohaline surface buoyancy forcing and interior diapycnal/diabatic mixing from internal waves and eddies. In the Atlantic, warm and saline waters flow northward all the way from the Southern Ocean into the Labrador and Nordic Seas. By contrast, there is no deep-water formation in the North Pacific, and its surface waters are fresher. Deep waters formed in the Southern Ocean become denser and thus spread in deeper levels than those from the North Atlantic. Note the small, localized deepwater formation areas in comparison with the widespread zones of mixing-driven upwelling. Wind-driven (residual) upwelling occurs along the Antarctic Circumpolar Current (ACC). (Kulhbrodt *et al.*, 2007)

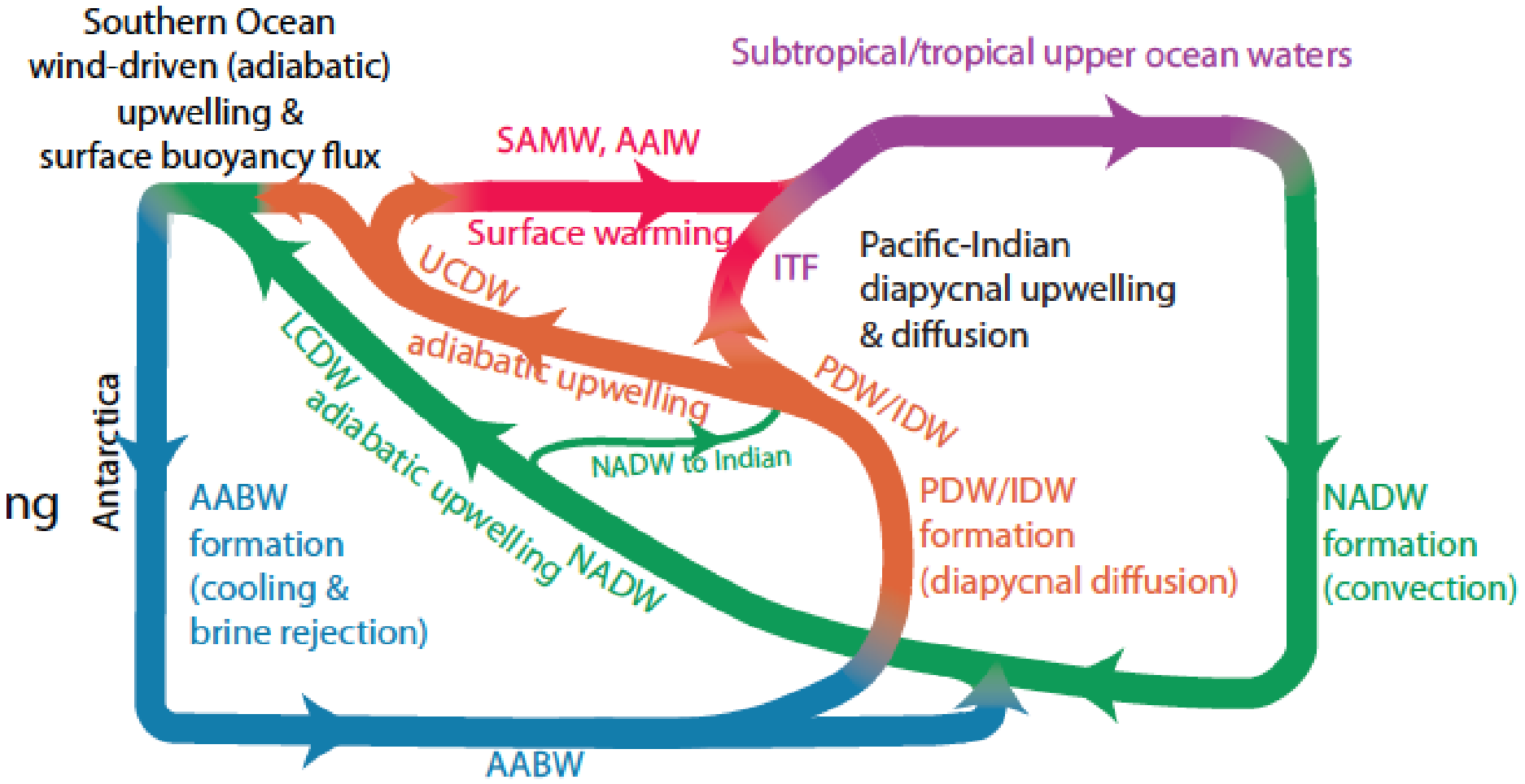

Schematic of the overturning circulation in a two-dimensional view ($i.e.$, the meridional plane, as with the previous OGCM $\Phi(y, z)$), with important physical processes listed, including NADW and AABW cells, and upwelling in the Southern, Indian and Pacific Oceans. (Talley, 2013)

.

Concept: Since the beginning of the European age of global exploration, with attendant, accumulating hydrographic profiles, "descriptive" oceanographers have attempted to diagram the global circulation in relation to identified water masses with distinctive thermodynamic and chemical properties.

This is an ill-posed inferential problem (a.k.a. inverse problem) that attempts to reconcile material distributions with the circulation and mixing in a steady-state advection/diffusion equation with interior sources and sinks. It has qualitative validity as a not-inconsistent reconstruction from observed geographical regularities, but its quantitative validity is unknown and probably unknowable.

A quantitative alternative is to diagnose the advective and parametrized mixing fluxes across some web of interior boundaries using an OGCM solution, but that of course is not fully verifiable.

Given the chaotic nature of oceanic trajectores at all scales, this type of diagram, though popular, is based on a falsely simple conception of material movement.

6. Thermohaline Circulation (THC): Buoyancy Forcing

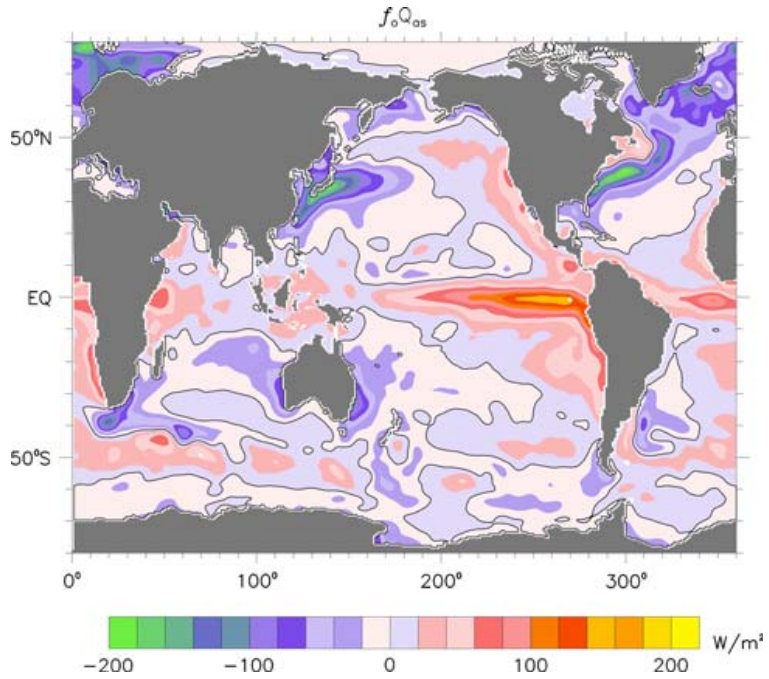

Mean surface heat flux, positive into the ocean, and colored at 20 W m^{-2} intervals.

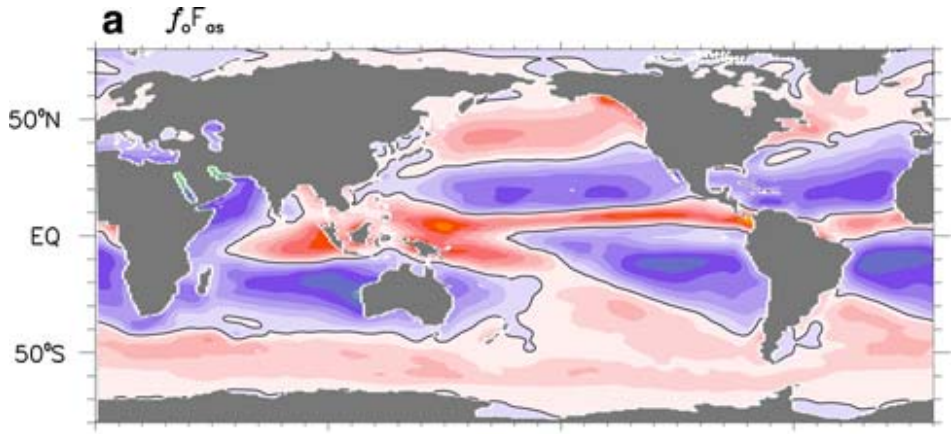

Mean surface water flux, positive into the ocean, and colored at 10 mg m/2 s^{-1} intervals.

Notice the opposite tendencies for buoyancy forcing: tropical/subtropical heating and salinification *vs.* subpolar/polar cooling and freshening. These are repeated figures from Large and Yeager (2009).

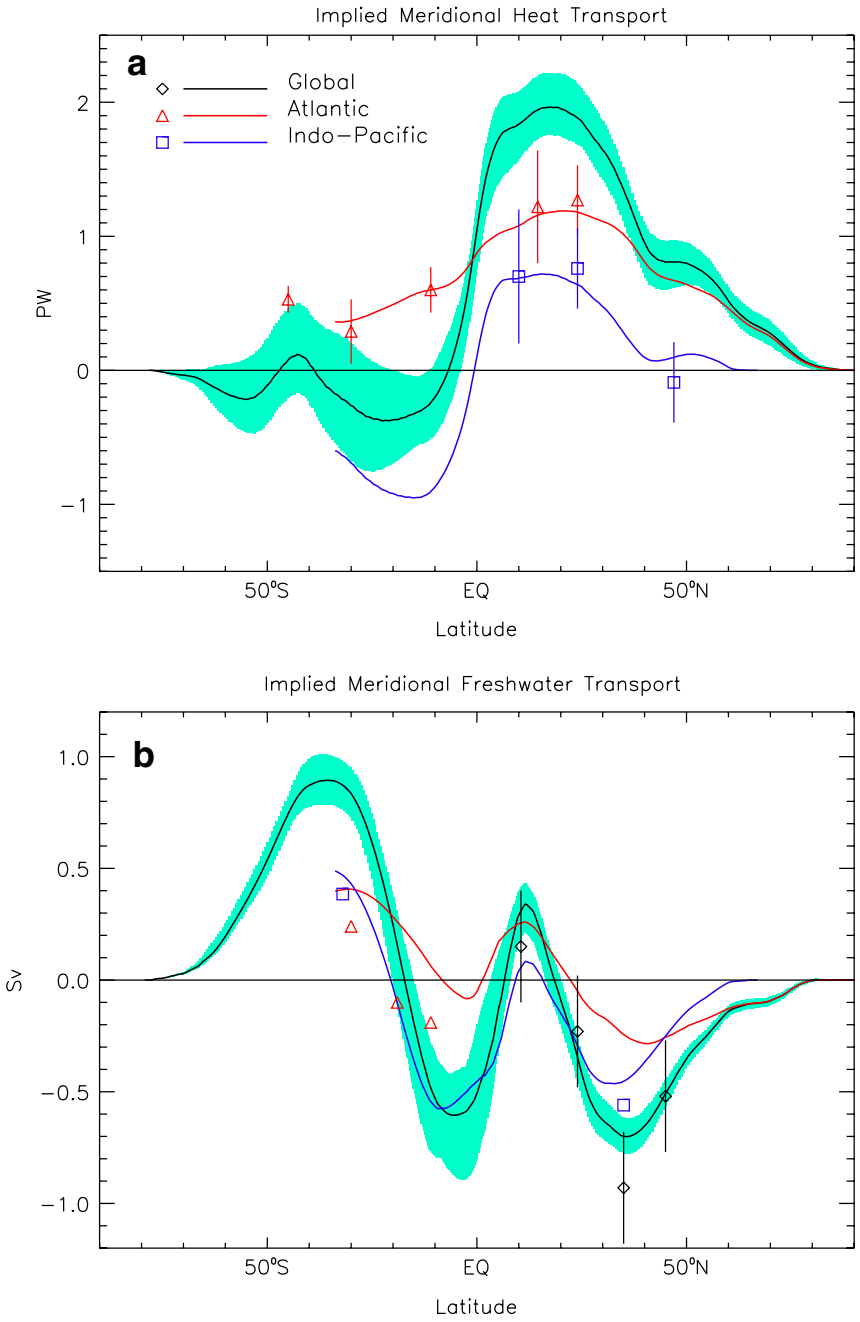

Northward ocean transports of (a) heat in PW and (b) freshwater in Sv. (Large and Yeagar, 2009)

Meridional Thermohaline Transport by Currents

Heat balance for zonal and depth integrated heat content:

$$\frac{d}{dt}\,\rho_0 C_p \int_{x_w}^{x_e}\int_{-h}^{0} dx\,dz\,T \;=\; -\,\partial_y \mathcal{H} + \int_{x_w}^{x_e} dx\,Q\,,$$

where $\mathcal{H}$ is the meridional oceanic heat flux by currents. In equilibrium the left-side is zero, and $\mathcal{H}$ is diagnosed from measurements of Q.

Analogous relations occur for the integrated freshwater content balance and its meridional flux.

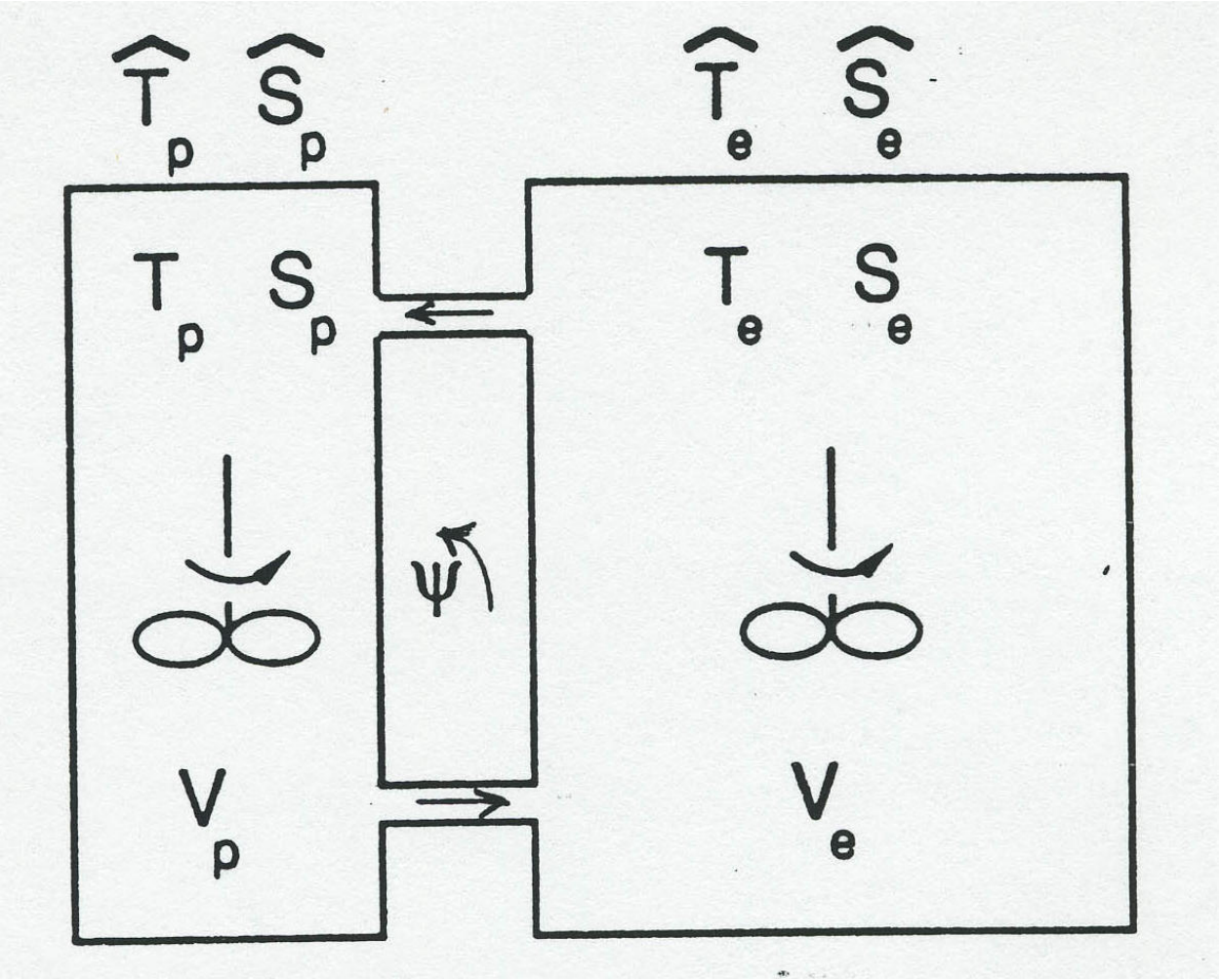

Configuration for a "conceptual" model system with equatorial and polar "box" volumes. Each box has T and S exchanges with its reservoir values (surface flux); is internally strongly stirred (turbulent mixing); and has an exchange between two boxes at a rate Ψ proportional to their density difference, $-\tilde{\alpha}(T_e - T_p) + \tilde{\beta}(S_e - S_p)$ (circulation). Remarkably, when the reservoir $\hat{T}$ and $\hat{S}$ values have opposing density effects, there are two different steady circulation modes that are interpreted as thermally-induced polar sinking (TH) and salinity-induced equatorial sinking (SA). It is likely that both have occurred in Earth's history. (Stommel, 1961)

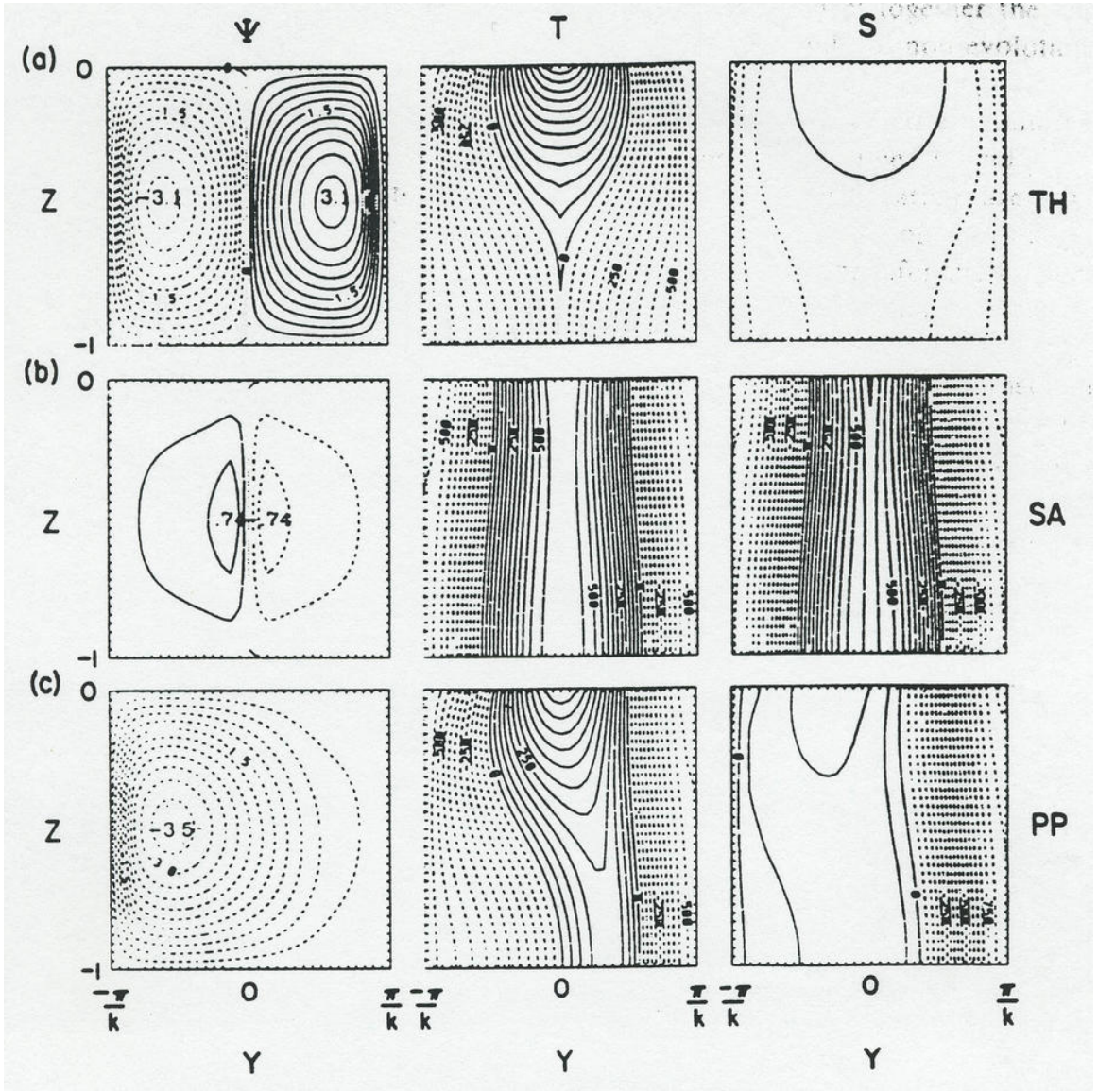

Multiple steady states in a 2D (y, z) "whole Earth" fluid model with surface Q and $\mathcal{F}$ acting to make the central (equatorial) region warm and salty. Ψ ($i.e.$, Φ) is the MOC streamfunction. The states are TH with thermally-induced polar sinking in both hemispheres and a well defined thermocline, SA with salinity-induced sinking at the equator and a weak circulation and almost no pycnocline, and PP with a pole-to-pole circulation with polar sinking in only one hemisphere, as in the modern Atlantic. (Thual and McWilliams, 1992)

7. Abyssal Circulation

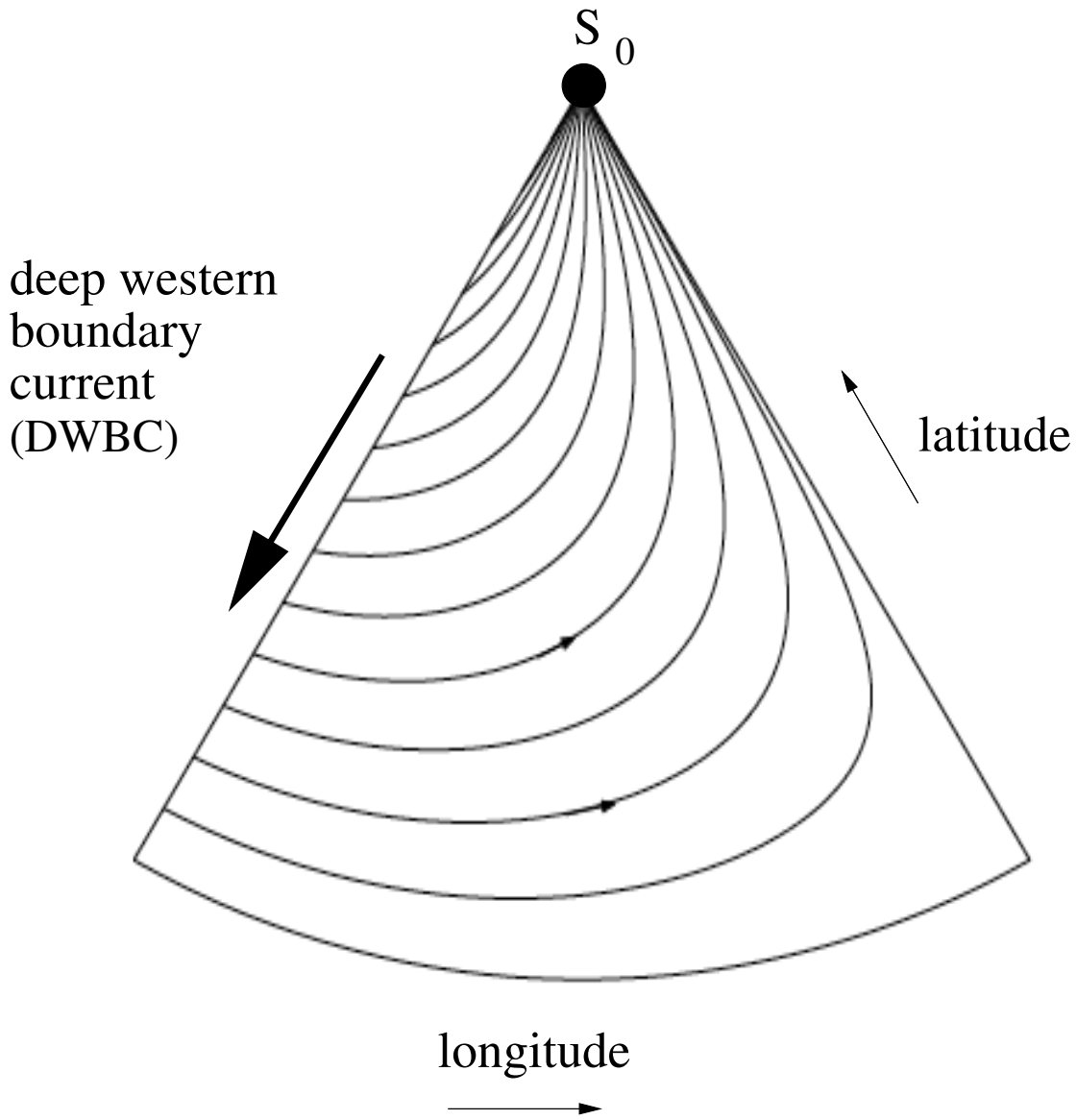

Horizontal interior circulation in a model of an abyssal layer of uniform density in a hemispherical sector. The forcing is a downward point volume flux S_0 at the north pole, mimicking deep convection and bottom-water formation, with a balancing uniform upwelling velocity $w_0 = S_0/Area$ everywhere else. The interior dynamics are planetary-geostrophic and incompressible. The interior flow is everywhere poleward and eastward, implying the existence of a deep western boundary current (DWBC) to close the horizontal circulation. The DWBC transport exceeds S_0 at high latitudes because of recirculation. (Stommel and Arons, 1960)

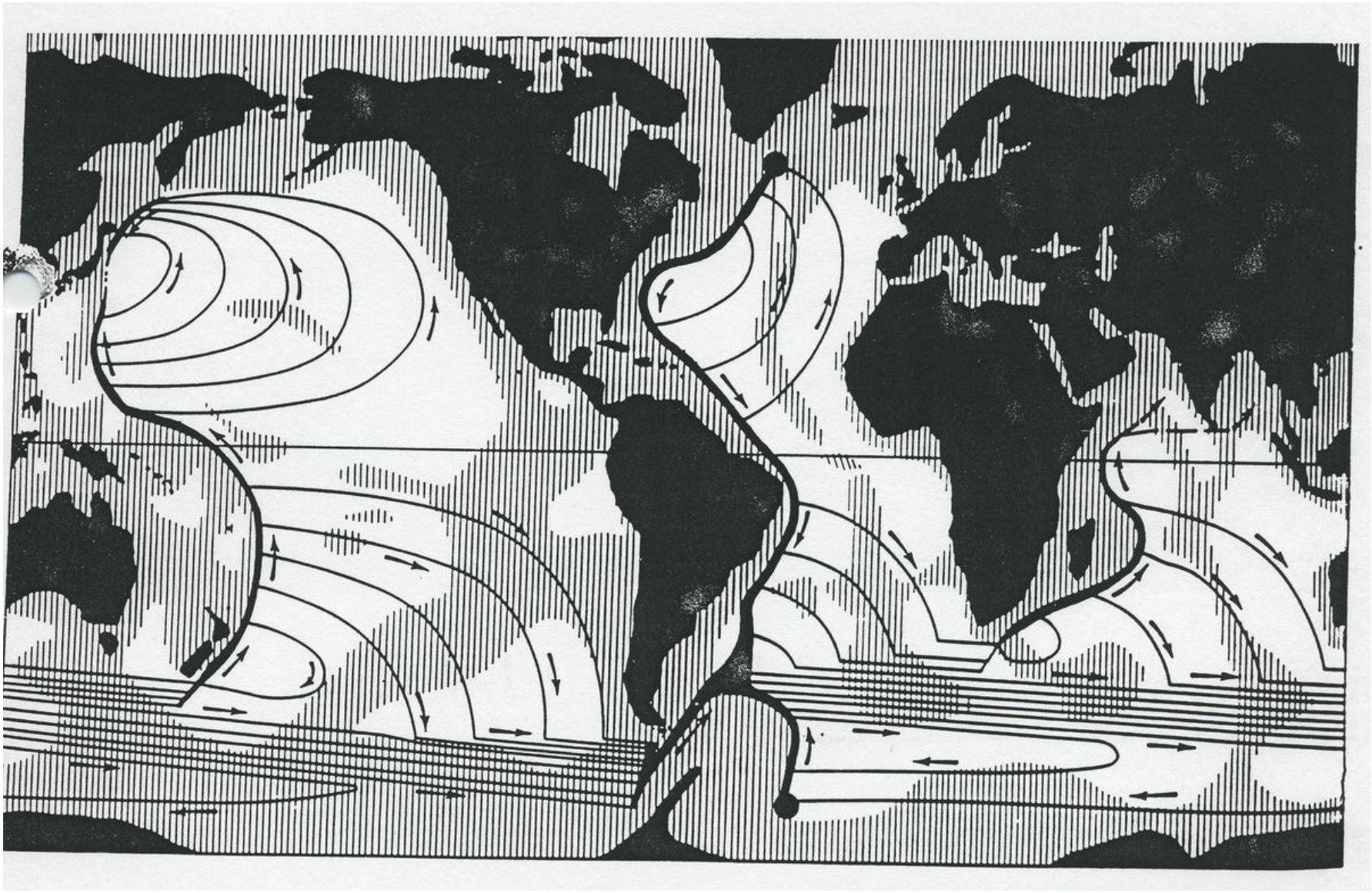

Ansatz for the global mean abyssal circulation based on specifying three numbers: the North Atlantic and Antarctic downward volume fluxes (each 20 Sv) and the ACC horizontal transport (50 Sv below 2000 m depth). Notice the DWBCs. Except for the ACC part, this flow conforms to the Stommel-Arons model deformed to match basin shapes (Stommel, 1958). This model, like the previous gyre in a rectangle and box model of thermohaline circulation, is not consistent in detail with measurements & OGCM solutions but it is a first, simplest "paradigm" for the phenomenon.

THC and Water Masses: North Atlantic Deep Water (NDW) Formation

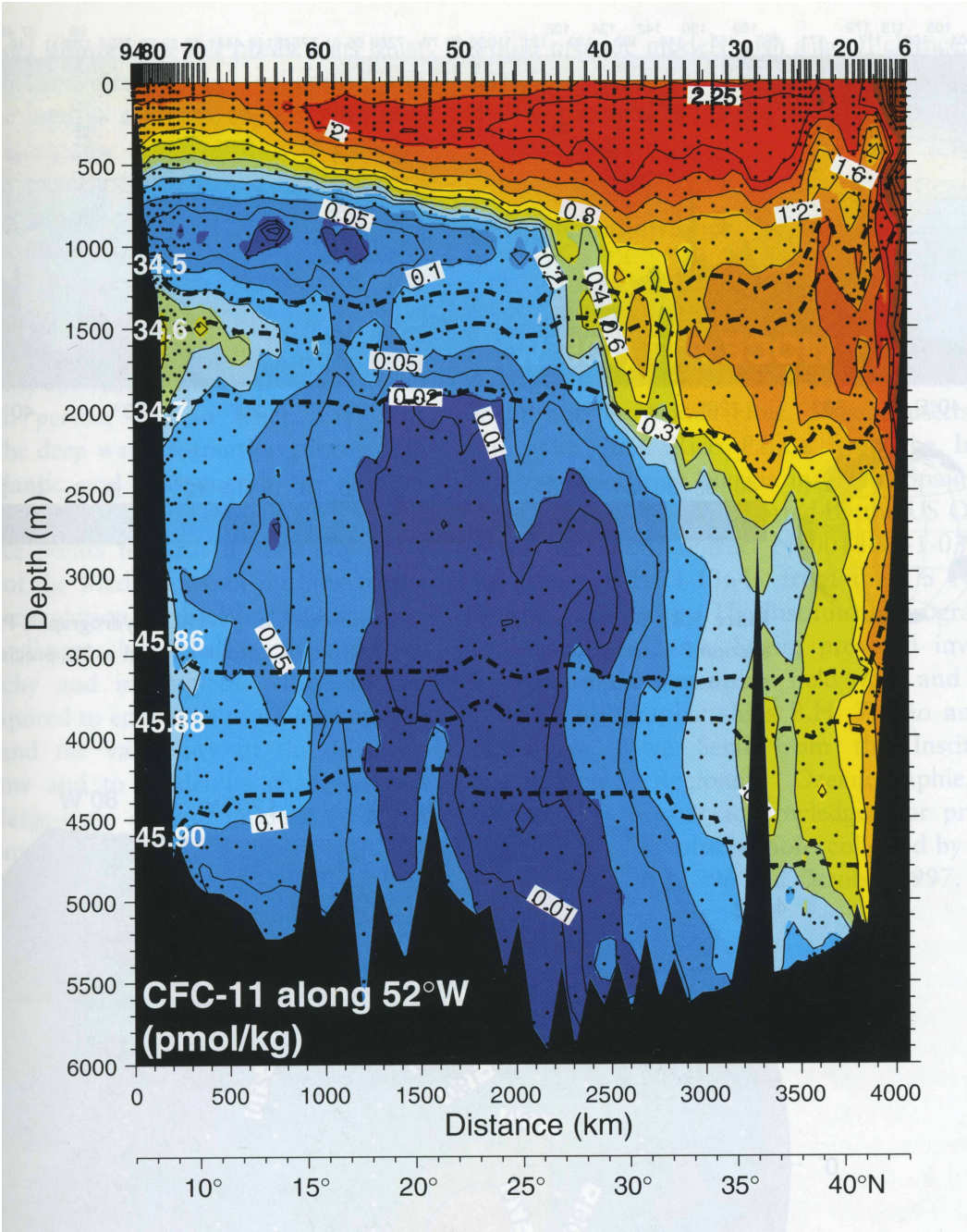

Concentration of CFC-11 along a meridional section in the North Atlantic, whose presence indicates gas exchange with the atmosphere since the 1950s. Note the penetration of young water in the subpolar region, indicative of NADW formation. (Schlosser *et al.*, 2001)

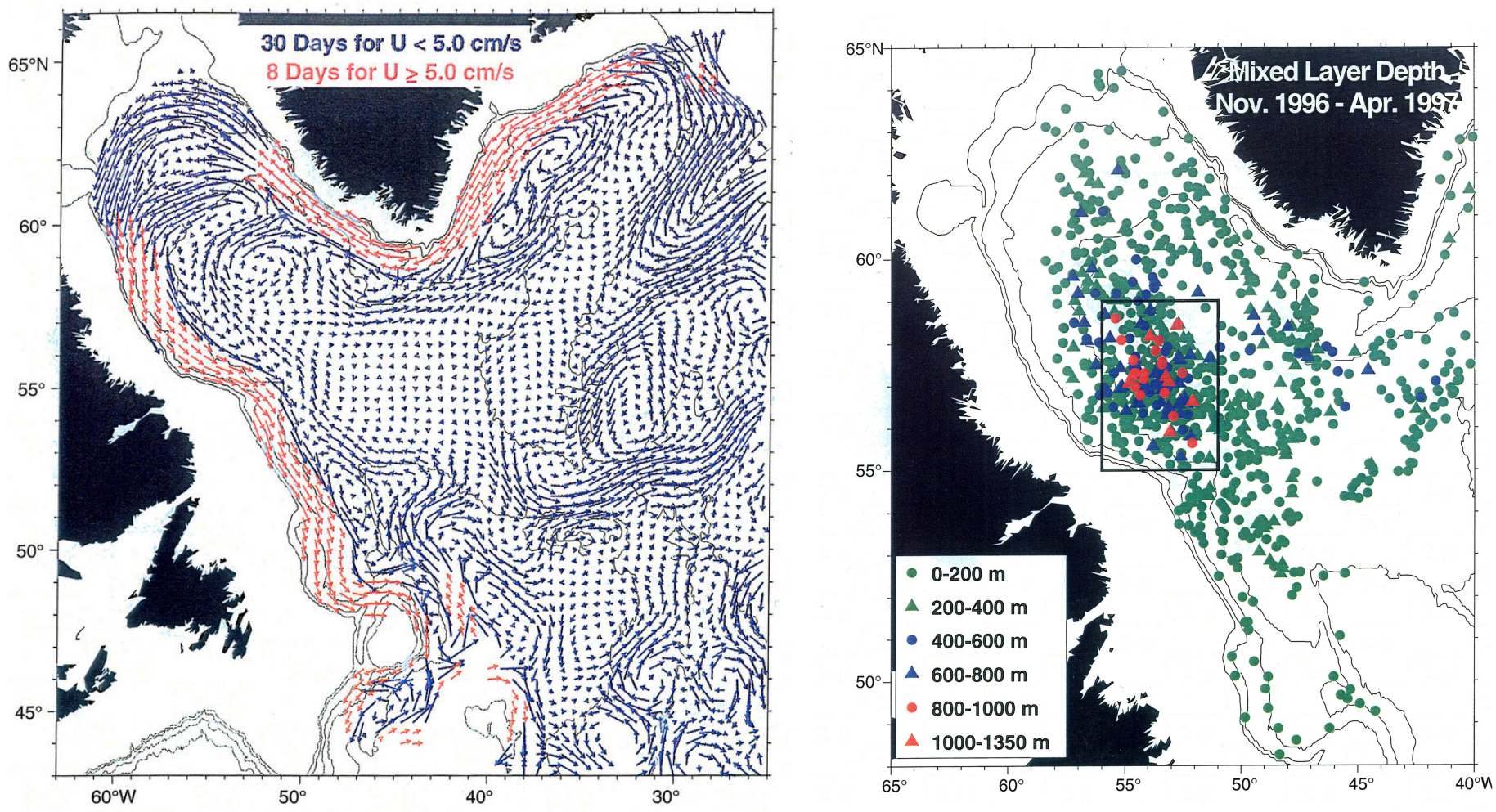

(Left) Mean circulation of the Labrador Sea and Irminger Basin at 700 m depth shown as lateral displacements with different colors for different time intervals. (Right) mixed layer depth h_{ML} [m] in the Labrador Sea during winter 1996-97. Measurements were made with profiling floats. The cyclonic subpolar gyres on both sides of Greenland induce geostrophic uplift of central-basin isopycnals as a "pre-conditioning" with reduced density stratification favorable to deep convection by surface cooling, hence larger h_{ML}. Notice the strong WBCs around the rim of this topographically complex basin. The net result is newly formed NADW. (Lavender $et\ al.$, 2000 & 2002)

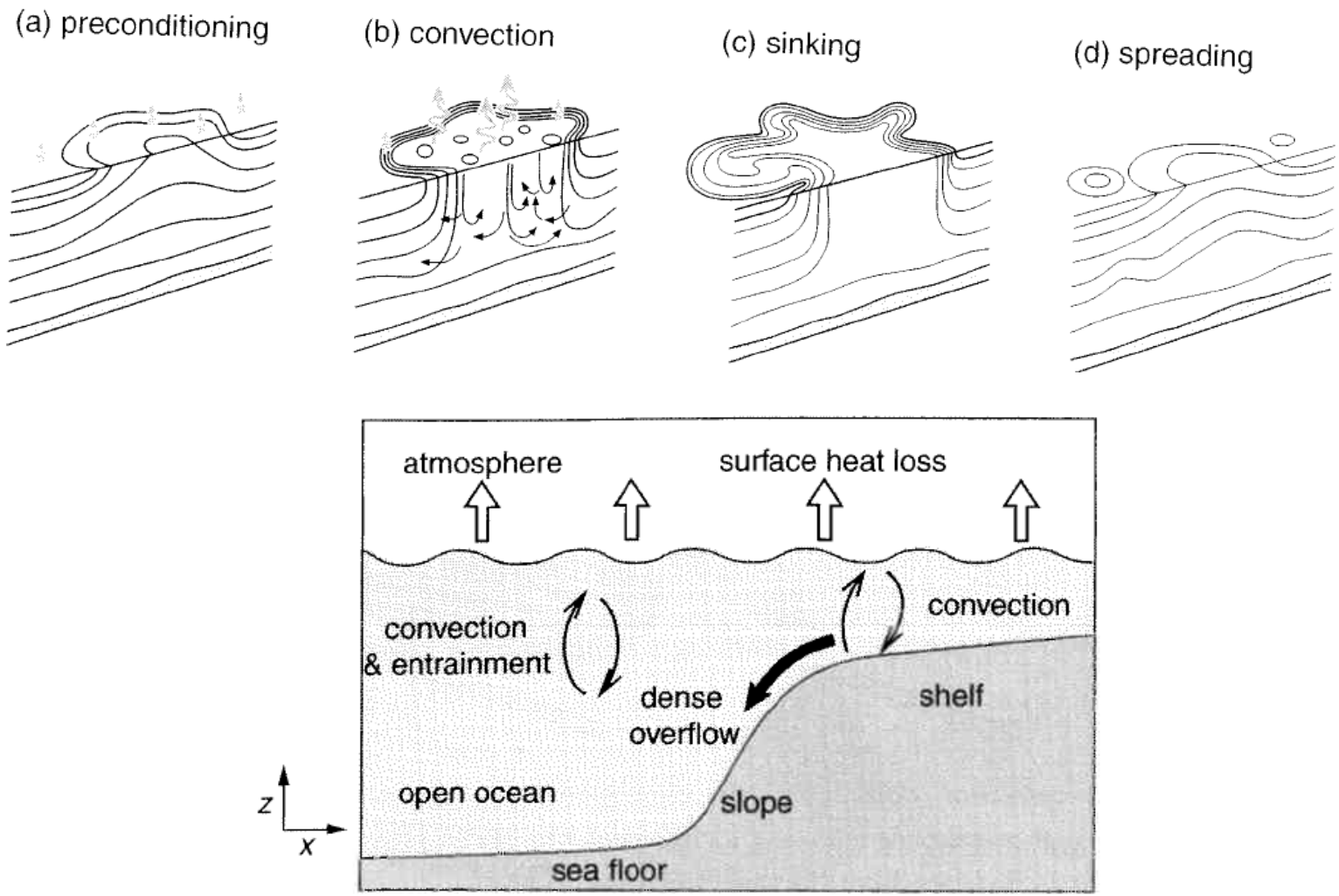

Cartoons of the formation processes of abyssal water: (top) deep convection in the open ocean, where baroclinic instability and eddy-induced advection play an important role in the "sinking" phase; (bottom) convection of dense water on a continental shelf, followed by slope gravity currents into the abyss. The top is more relevant to the Nordic and Labrador Seas, while the bottom is more relevant to the Antarctic shelfs in the Ross and Weddell Seas.

THC: Deep Western Boundary Current

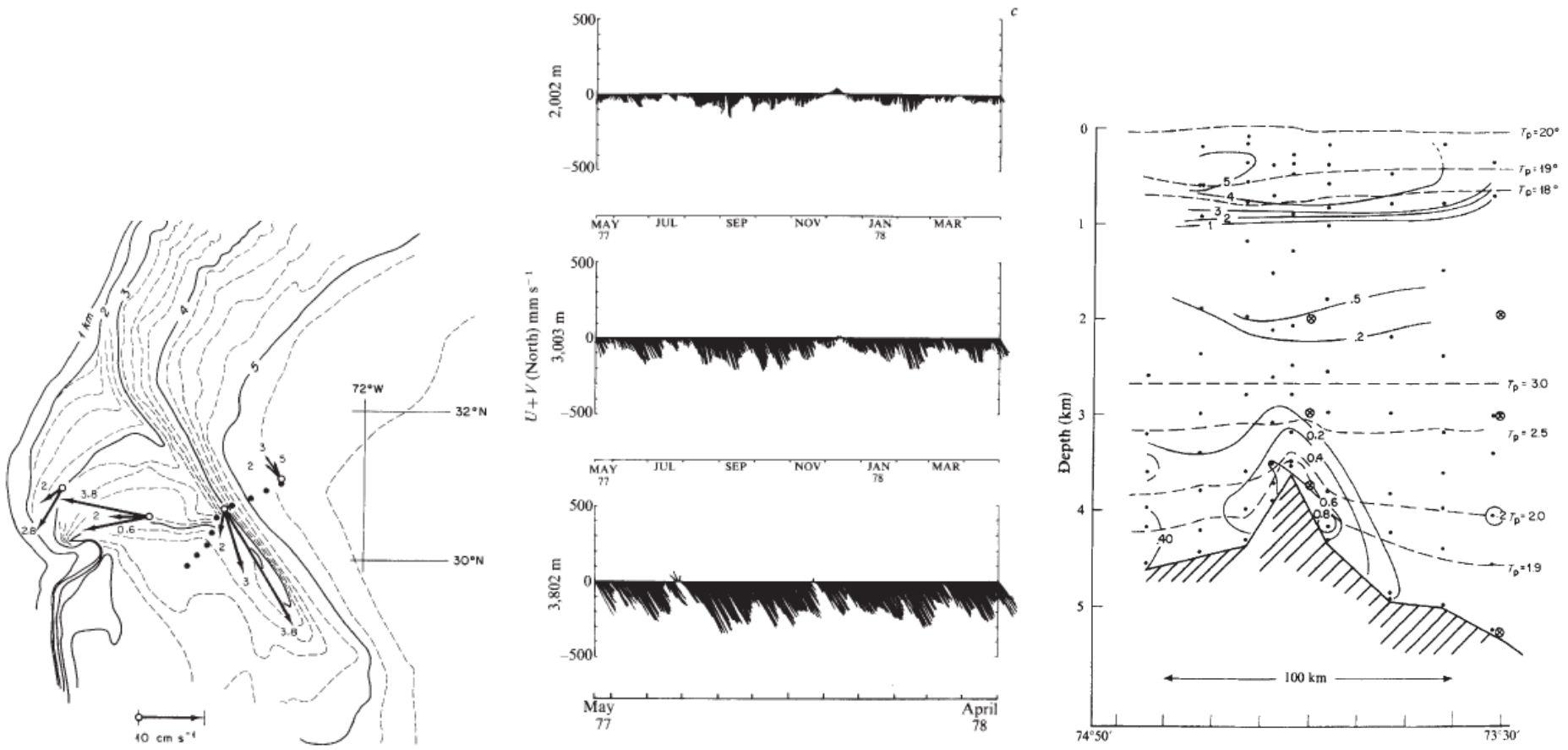

Measurements of the Deep Western Boundary Current (DWBC) in the abyssal subtropical North Atlantic with time mean velocity vectors at the labeled depths [km]. This is the southward branch of the NADW thermohaline circulation. (Right) Array location off the east coast of the U.S. (Middle) 1-year time series for horizontal velocity vectors at the central mooring at three depths. (Right) Hydrographic section along the array for tritium concentration [TU $= {}^{3}$H atoms per 10^{8} ^{1}H atoms] in (solid contours) and potential temperature [C] (dashed); it shows the DWBC below 3 km depth carries recently ventilated water southward. (Jenkins and Rhines, 1980)

THC: Sea Ice and Antarctic Bottom Water (AABW) Formation

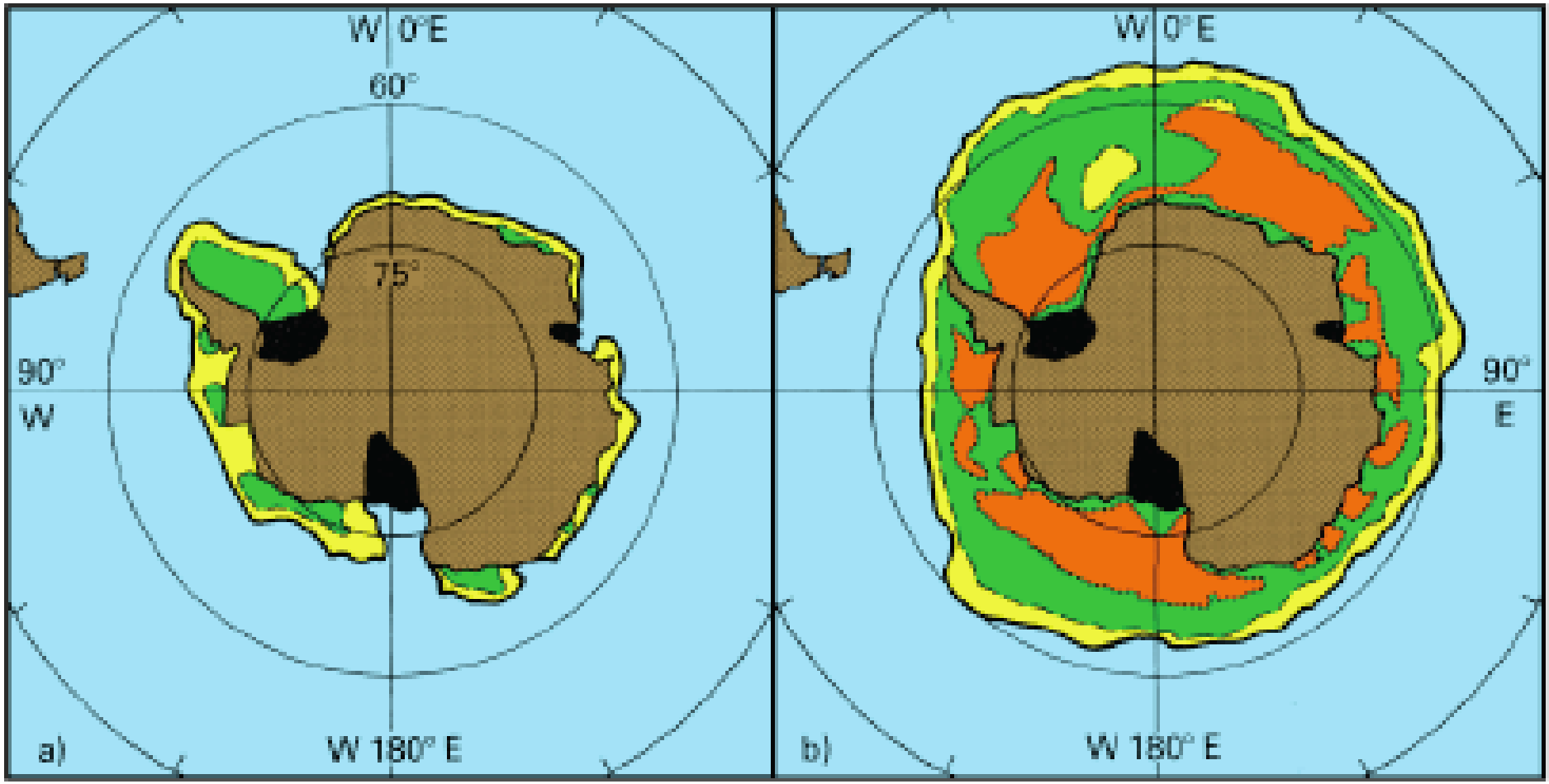

Mean seasonal ice conditions in Antarctica, based on satellite data for 1973-1976: (a) late summer (February), and (b) late winter (October). Black areas indicate ice shelf (grounded on ocean floor). The solid, broken, and doted lines indicate ice areal coverages of 15%, 50%, and 85%. Sea ice plays an important role in establishing the (T, S) properties of surface water that sinks to the bottom along the Antarctic edges and spreads globally as Antarctic Bottom Water (AABW).

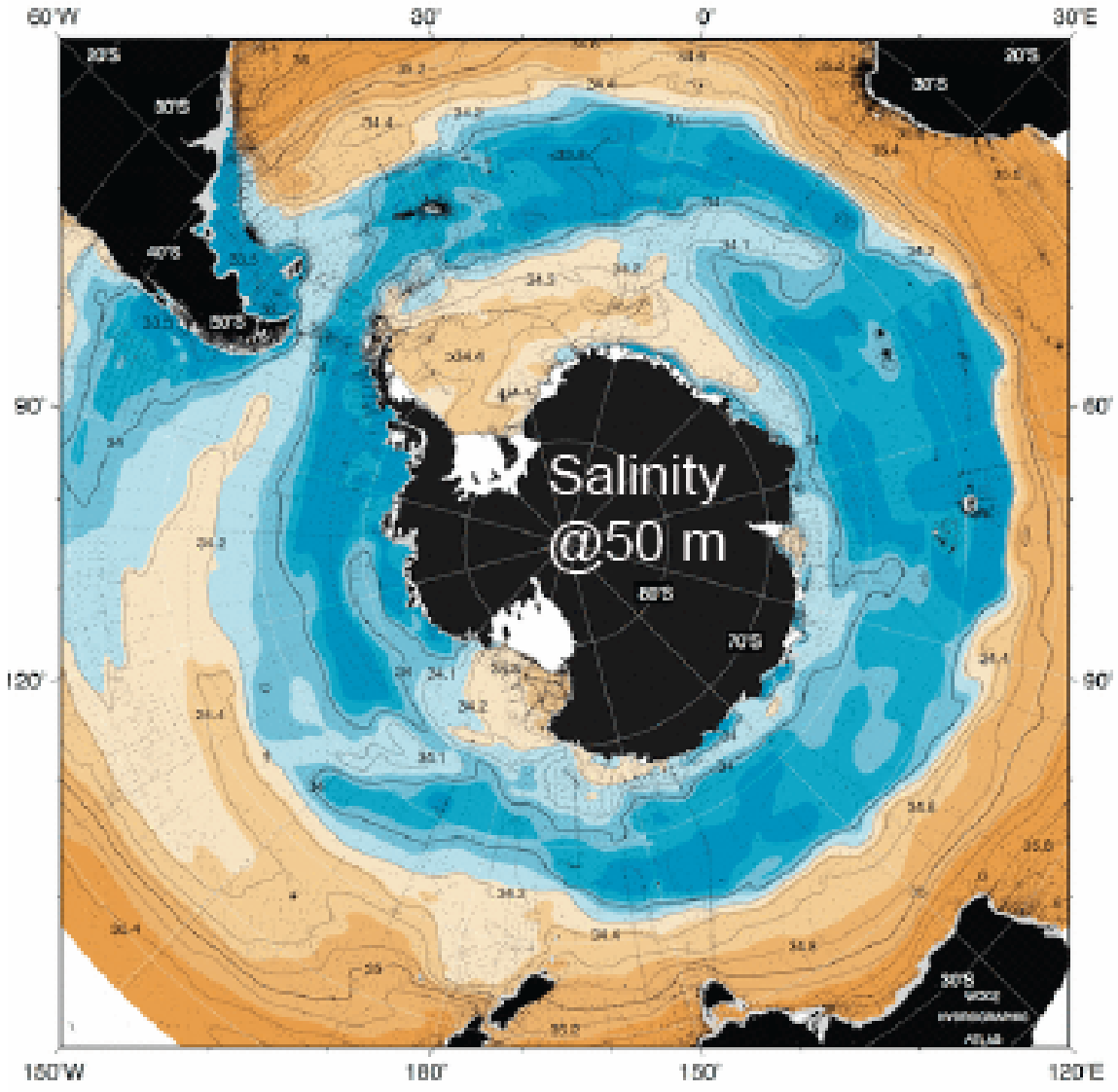

S in Antarctic surface waters reflects the southward import of salty NADW, precipitation, ice melt, and brine rejection during sea ice formation. The dense, salty water in the Weddell (30W) and Ross (140W) Seas are principal sites for AABW formation and sinking.

8. Meridional Overturning and Water Mass Geography

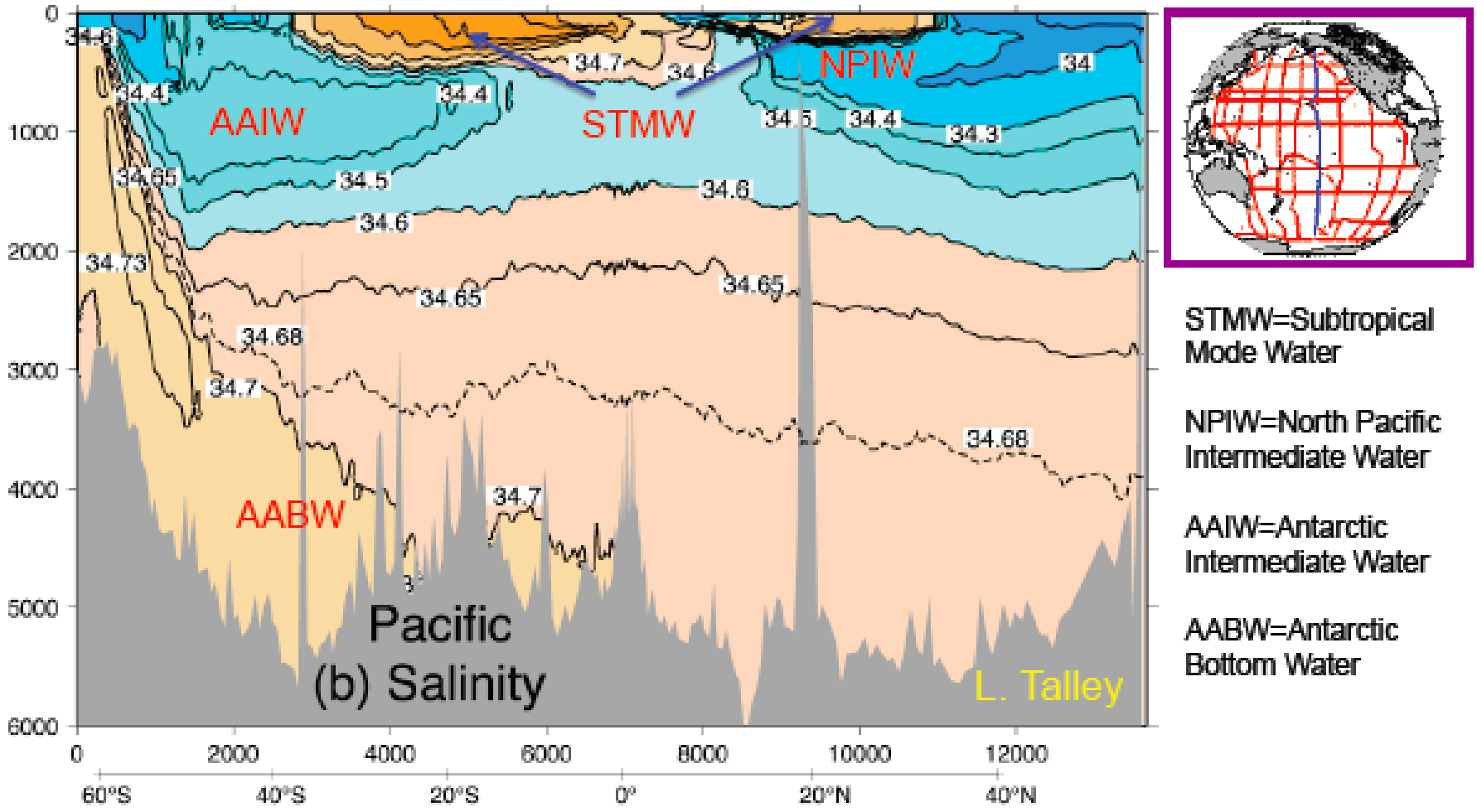

Salinity [PSU] section in the Pacific from WOCE data along the P16 line in the inset. The labels are the water mass types. Over most of the section S has a weak dynamical influence, compared to T, but it tracers the path of surface waters into the interior. The STMW are trapped pools above the deep pycnoclines in subtropical gyres created by wintertime surface mixing. In the Pacific abyssal water (AABW) comes only from the south.

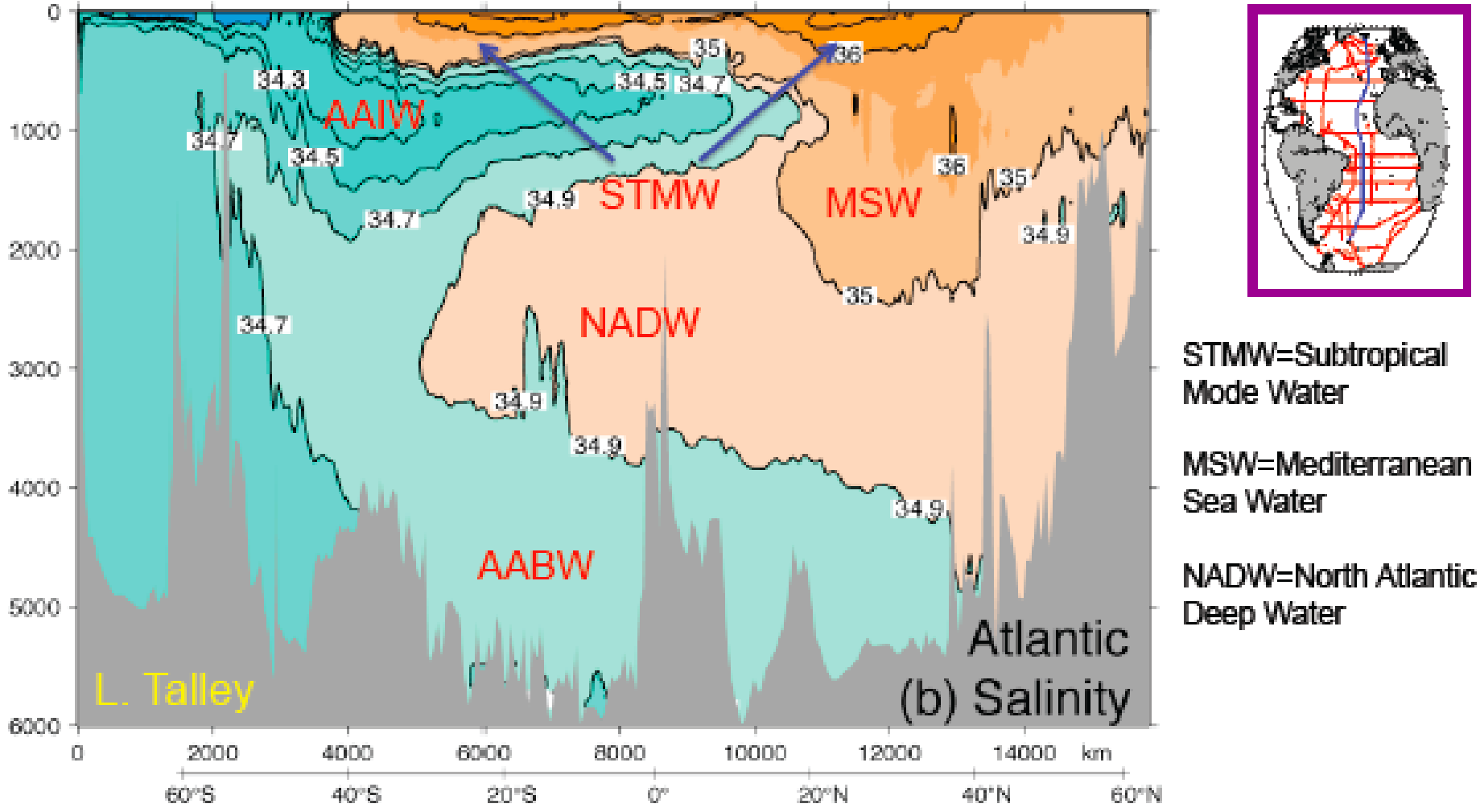

Salinity [PSU] section in the Atlantic from WOCE data along the A16 line in the inset. The labels are the water mass types. AAIW and AABW are defined in the preceding slide. They are labeled by their water mass type. MSW enters the Atlantic through Gibraltar Strait and arises from high evaporation within the Mediterranean basin. Abyssal water comes from both the north (NADW) and south (AABW).

Southern Ocean Water Masses

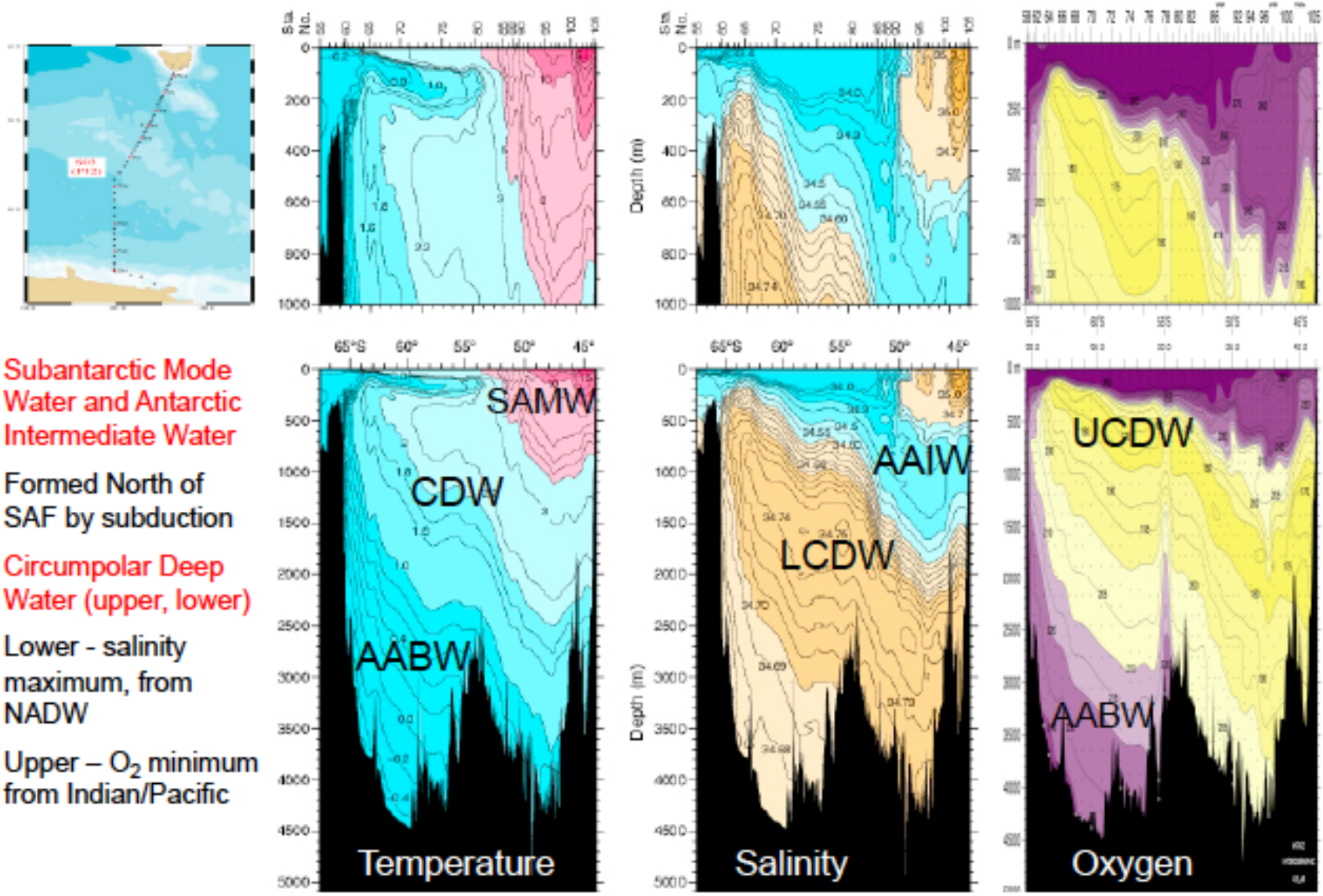

Meridional sections of T, S and O_2, with a zoom of the upper 1 km in the top row. The Subantarctic Front (SAF) is an upper-ocean water-mass boundary in T and S. Circumpolar Deep Waters (CDWs) are mixtures around the ACC of other waters with surface sources.

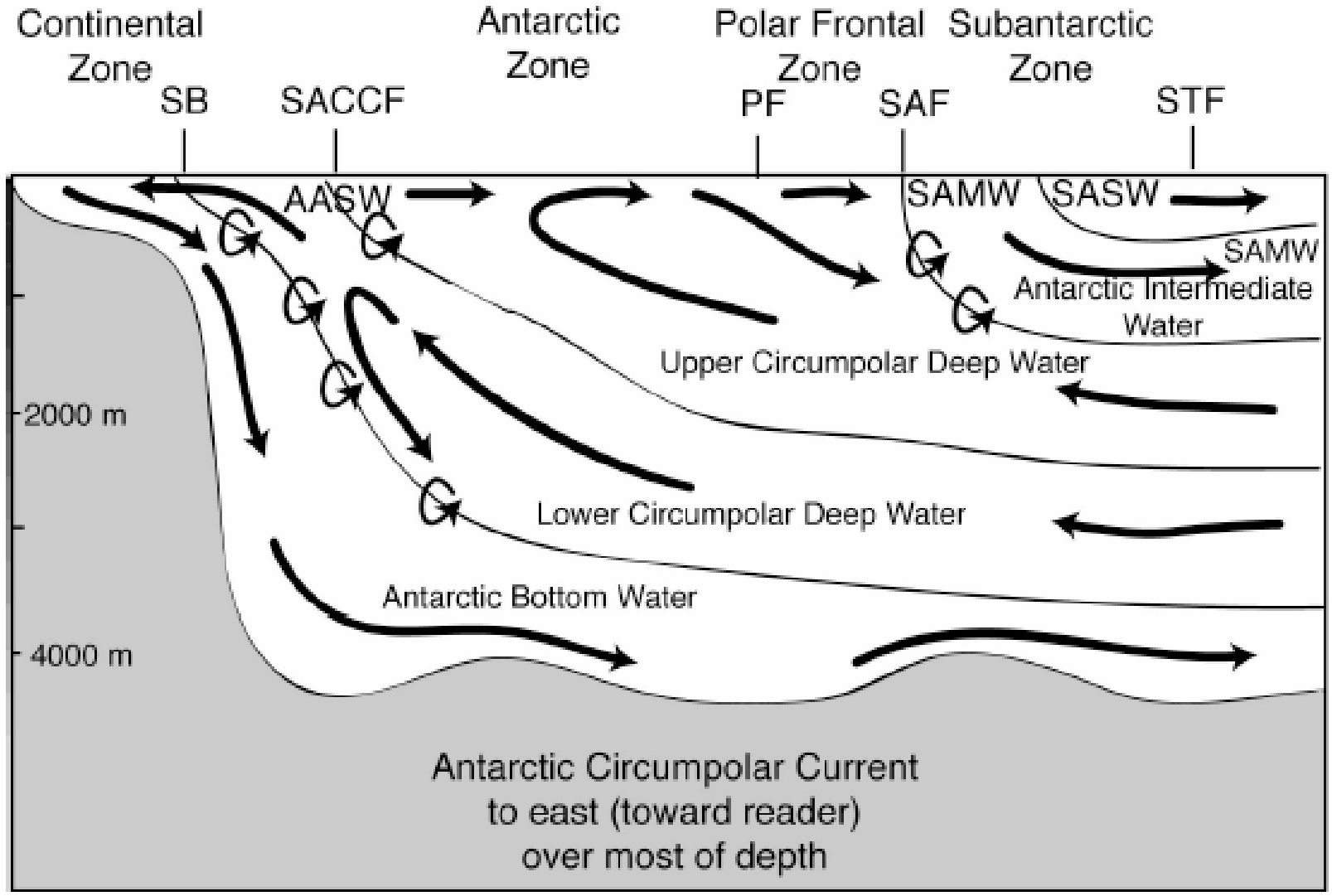

Sketch of the MOC in the Southern Ocean, mostly inferred from water mass analysis. Notice that the core of the ACC is a place where substantial amounts of deep water rise back to the surface. It includes an inference of the deep overturning circulations in this sector: the upper cell (UCDW $\rightarrow$ SAMW and AAIW) and the lower cell (AABW $\rightarrow$ LCDW). This can be compared with the previous OGCM MOC slide, *i.e.*, the Lagrangian residual circulation that advects material concentrations. This circulation is difficult to measure directly.

Global Radiocarbon Section

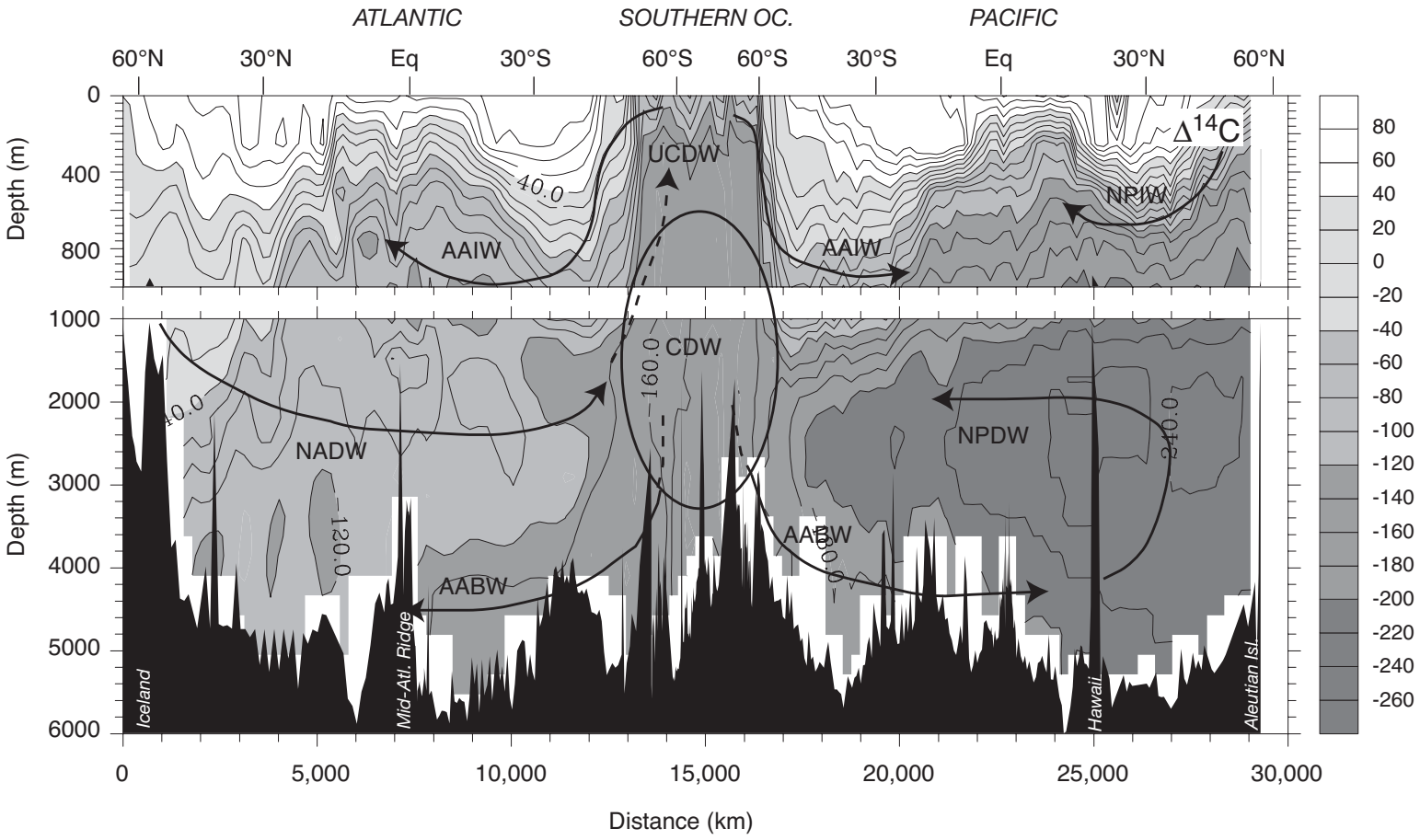

Concentration of the radiocarbon ^{14}C isotope in total CO_2 (DIC) along a section from Iceland to Alaska. Values are normalized to a common pre-industrial atmospheric 14C/12C ratio and reported in permil units, so that a -100 permil value corresponds to $\approx$ 10% depletion relative to the atmospheric 14C/12C ratio. Surface and thermocline values above zero are due to uptake of $^{14}CO_2$ from nuclear weapons testing in the 1950's. The decreasing ^{14}C from the North Atlantic to the Southern Ocean, and from the Southern Ocean to the North Pacific reflects the radioactive decay along the flow paths of NADW and AABW. (Sarmiento and Gruber, 2006)

Global Water Mass Sources

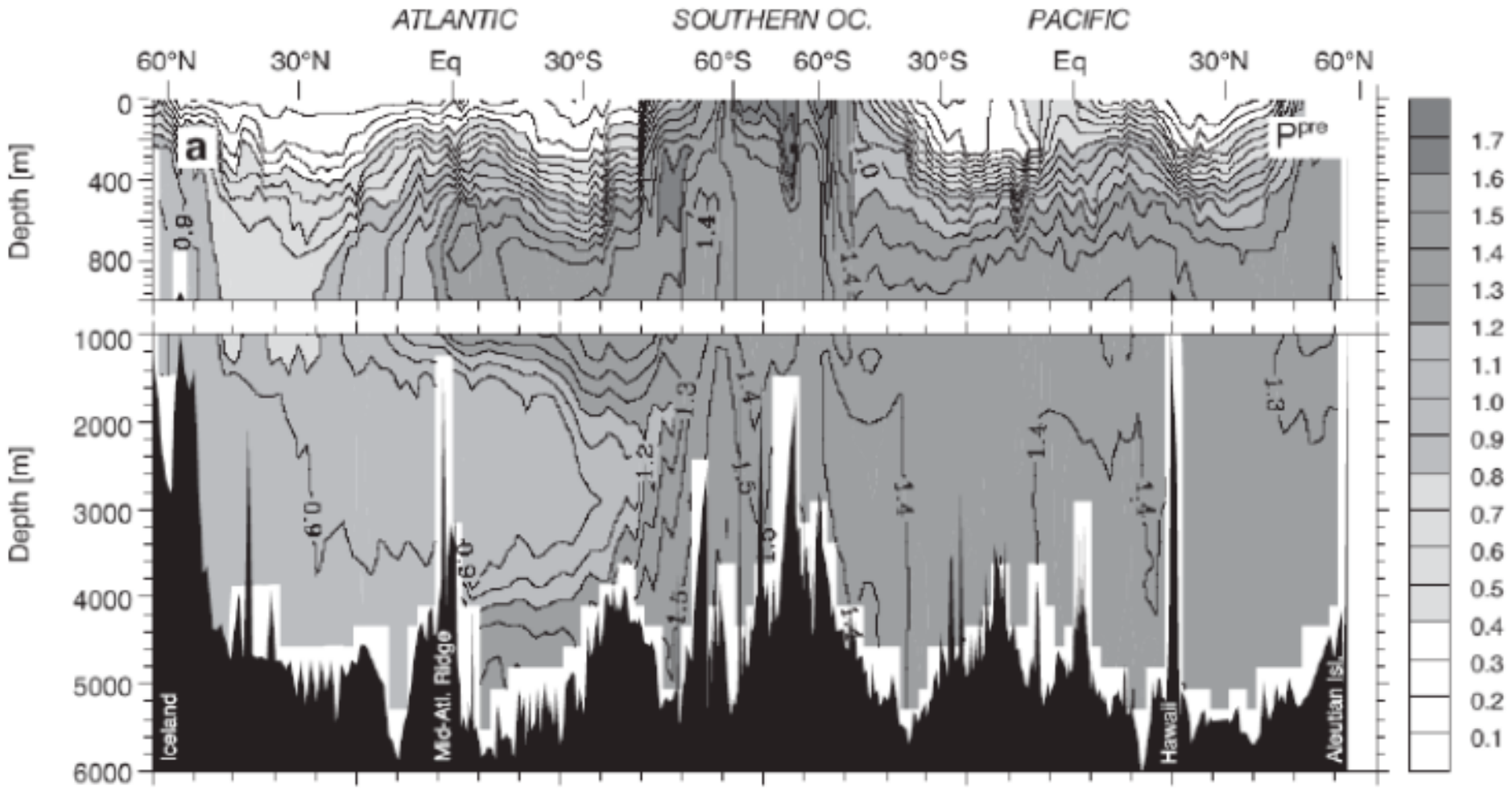

This is "preformed phosphate" [μmol/kg], $P_{pre} = PO_4 + \Delta O_2/150$. a nearly conservative tracer. It is set in the surface layer where O_2 is saturated, and it is unchanged along its interior pathway as organic matter remineralizes into phosphate by oxidation with the indicated elemental ratio 1/150 ($i.e.$, a Redfield ratio, typical for seawater) and ΔO_2 decreases — as will be further explained later. It provides a measure of the contribution of NADW versus AABW to abyssal water masses. The Antarctic surface-layer source is dominant in a larger volume than the North Atlantic source, even though its deep-water formation rate is probably not quite as large.

Abyssal Radiocarbon Age

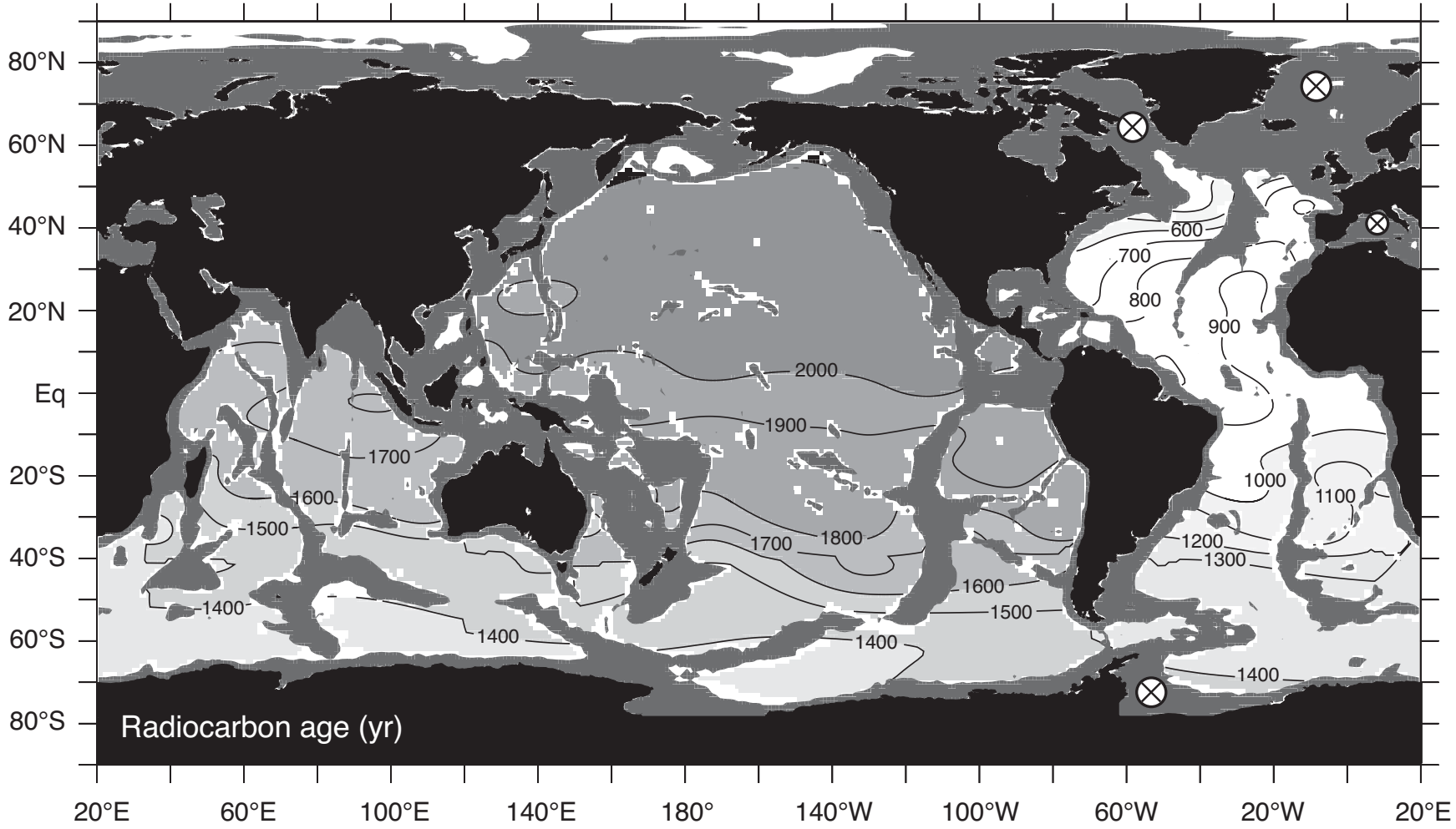

Map of ^{14}C-age (years) at 3500 m depth computed from ^{14}C measurements and a radioactive decay constant of 1/8300 years (half-life 5700 years). (*cf.*, the ^{14}C concentration slide in the Measurements lecture.) The ages indicate that the deep flow from the North Atlantic to the North Pacific has a time-scale of $>$ 1000 years. Age is a product of mixing and advection, so for old water the age is generally less than the advection time by the mean circulation alone because of mixing with surrounding younger waters. (Sarmiento and Gruber, 2006)

References

Garcia, *et al.*, 2005: *World Ocean Atlas*. NOAA Atlas, NESDIS.

Gent, P., and J. McWilliams, 1990: Isopycnal mixing in ocean circulation models. *J. Phys. Ocean.* **20**, 150-155.

Jenkins, W.J., and P.B. Rhines, 1980: Tritium in the deep North Atlantic ocean. *Nature* **286**, 877-880.

Karsten, R., and J. Marshall, 2002: Testing theories of the vertical stratification of the ACC against observations. *Dyn. Atmos. Oceans* **36**, 233-246

Kuhlbrodt, T., A. Griesel, M. Montoya, A. Levermann, M. Hoffman, and S. Rahmstorf, 2007: On the driving processes of the Atlantic meridional overturning circulation. *Reviews of Geophysics* **45**, 2004RG000166.

Large, W. and S. Yeager, 2009: The global climatology of an interannually varying air-sea flux data set. *Climate Dyn.* **33**, 341-364.

Lavender, K., R. Davis, and B. Owens, 2000: Mid-depth recirculation observed in the interior Labrador and Irminger seas by direct velocity measurements. *Nature* **407**, 66-69. & . . . 2002: Observations of open-ocean deep convection in the Labrador Sea from subsurface floats. *J. Phys. Ocean.* **32**, 511-526.

Marshall, J., 1984: Eddy-mean-flow interaction in a barotropic ocean model. *Q. J. Roy. Met. Soc.* **110**, 573-590.

Qiu, B., and R. Huang, 1995: Ventilation of the North Atlantic and North Pacific: Subduction versus obduction. *J. Phys. Ocean.* **25**, 2374-2390.

Sarmiento, J., and N. Gruber, 2006: *Ocean Biogeochemical Dynamics*. Princeton Press.

Schlosser, P., *et al.*, 2001: Transformation and age of water masses. In: *Ocean Circulation and Climate*, G. Siedler, J. Church, and J. Gould (eds.), Academic Press, 431-452.

Stewart, Robert, 2008: *Introduction To Physical Oceanography.*
`http://oceanworld.tamu.edu/resources/ocng_textbook/PDF_files/book_pdf_files.html`

Stommel, H., 1948: The westward intensification of wind-driven ocean currents. *Trans. Amer. Geophys. Union* **29**, 202-206.

Stommel, H., 1958: The abyssal circulation. *Deep-Sea Res.* **5**, 80-82.

Stommel, H., and A.B. Arons, 1960: On the abyssal circulation of the world ocean. I Stationary planetary flow patterns on a sphere & II. An idealized model of the circulation pattern and amplitude in ocean basins. *Deep-Sea Res.* **6**, 140-154 & 217-233.

Stommel, H., 1961: Thermohaline convection with two stable regimes of flow. *Tellus* **2**, 244-268.

Talley, L. 2013: Closure of the global overturning circulation through the Indian, Pacific and Southern Oceans: schematics and transports. *Oceanography* **26**, 80-97.

Thual, O. and J. McWilliams, 1992: The catastrophe structure of thermohaline convection in a two-dimensional fluid model and a comparison with low-order box models. *Geophys. Astrophys. Fluid Dyn.* **64**, 67-95.